

Energy & Environmental Science

Accepted Manuscript



This is an *Accepted Manuscript*, which has been through the Royal Society of Chemistry peer review process and has been accepted for publication.

Accepted Manuscripts are published online shortly after acceptance, before technical editing, formatting and proof reading. Using this free service, authors can make their results available to the community, in citable form, before we publish the edited article. We will replace this *Accepted Manuscript* with the edited and formatted *Advance Article* as soon as it is available.

You can find more information about *Accepted Manuscripts* in the [Information for Authors](#).

Please note that technical editing may introduce minor changes to the text and/or graphics, which may alter content. The journal's standard [Terms & Conditions](#) and the [Ethical guidelines](#) still apply. In no event shall the Royal Society of Chemistry be held responsible for any errors or omissions in this *Accepted Manuscript* or any consequences arising from the use of any information it contains.

COMMUNICATION

A promising combination of brand-new silole-containing ladder-type heptacyclic arene and naphthobisoxadiazole moieties for highly efficient polymer solar cells

Cite this: DOI: 10.1039/x0xx00000x

Received 00th January 2012,

Accepted 00th January 2012

DOI: 10.1039/x0xx00000x

www.rsc.org/

Zhiyun Zhang,^{‡a} Francis Lin,^{‡a} Hsieh-Chih Chen,^{*a,b} Hung-Chin Wu,^c Chin-Lung Chung,^a Chien Lu,^c Shih-Hung Liu,^a Shih-Huang Tung,^d Wen-Chang Chen,^c Kentung Wong,^{*a} and Pi-Tai Chou^{*a}

We report a promising combination of brand-new silole-containing ladder-type heptacyclic arene and naphthobisoxadiazole moieties for highly efficient polymer solar cells. This new class of PSiNO polymer possesses great planarity and rigidity of backbone but has rather low-ordering framework. This unique feature facilitates the chains extension, leading to high hole mobility and hence high PCE of 8.37 % without further thermal annealing.

The discovery of polymer-based bulk heterojunction (BHJ) structures, in which polymer donor and fullerene acceptor are cast from a common solution to form a bicontinuous interpenetrating network for efficient exciton diffusion, charge separation and charge transport, has been lighting up the prospect for high efficiency polymer solar cells (PSCs). In recent years, combining electron-rich and electron-deficient moieties to form donor–acceptor (D–A) copolymers became a widely accepted strategy to develop low bandgap polymers. This is mainly due to their facile tunability of electronic structure via controlling the intramolecular charge transfer (ICT) from donor to acceptor moieties.^{1–10} In addition, vast numbers of studies in developing new photoactive materials, especially electron donating polymers,^{1–10} and device architecture innovation^{11–16} have brought about significant enhancement in power conversion efficiencies (PCEs), which has been achieved 8–9% for single-junction cells.^{3–6, 10, 12–15} In addition to the aforementioned methods, there have also been significant research efforts on developing inverted device structures, in which the charge collection of electrode is opposite to those of conventional configurations, to enhance the performance of solar cells and device air-stability.^{17,18}

This technique is very useful in its favorable vertical phase separation and concentration gradient in the active layer.¹⁹ Recently, incorporation of interfacial dipole layers for inverted PSCs has received much attention with proven ability of increasing the internal built-in potential, decreasing the serious resistance, and improving the charge extraction and collection through modifying the Fermi level alignment to either the $E_{F,h}$ of the donor material or the $E_{F,e}$ of the acceptor material for hole and electron transport towards the respective electrodes.^{14,17,20} Consequently, both interfacial contact resistance and undesired charge recombination are minimized, resulting in the enhancement of device performance.²¹ Although this efficiency still lags behind silicon-based inorganic devices, from chemistry point of view, the design and syntheses of various polymers are versatile such that the prospect for further improvement is brightening.

In this regard, a recent key target for organic-electronic materials should be ascribed to the extended π -conjugation of ladder-type polymer with coplanar geometry and structure rigidification by covalent fastening adjacent aromatic units in the polymer backbone. In this framework the π -system planarization facilitates π -electron delocalization to narrow the bandgap as well as suppresses rotational disorder about single bonds to reduce Marcus reorganization energies, both of which render facile exciton separation into free charge carriers.^{22–25} In this approach, benzo[1,2-*b*:4,5-*b'*]-dithiophene (BDT) and dithieno[3,2-*b*:2',3'-*d*]silole (DTS) are attractive for the donor units because of their good electron-donating ability, planar molecular structure and fine-tuning of structural modification.^{2,4,5, 8–10, 26–28} The D–A copolymers based on BDT or DTS show broad absorption, relatively low-lying HOMO energy

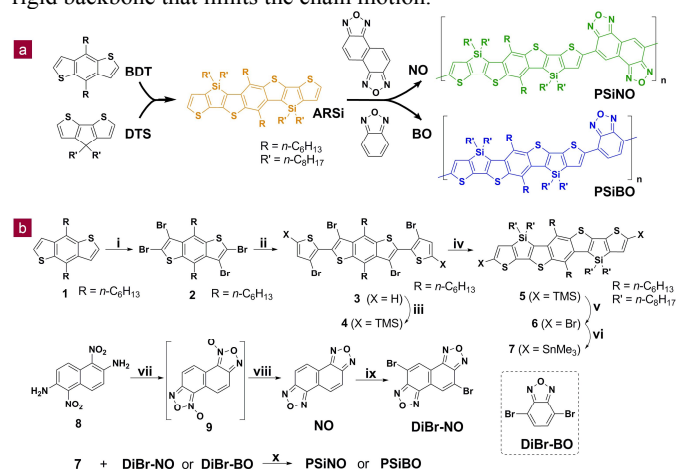
level and high hole mobility,^{2,4,5, 8-10, 26-28} indicating that BDT and DTS have emerged as attractive building blocks for highly efficient conjugated polymers. These results inspire us to hybridize BDT/DTS units into mutually fused structures to promote planarity and charge transport efficiency, which could provide an opportunity to tune the optoelectronic properties and expect to improve the photovoltaic performance.

In this communication, we report a straightforward synthetic methodology, for the first time, to prepare a series of brand-new D-A alternating copolymers shown in Scheme 1 and applied to PSCs. This ladder-type 5,11-dihexyl-4,4,10,10-tetraoctylbenzo[1,2-*b*:4,5-*b'*]bis-thieno[4",5"-*b'*:4"',5'''-*b'''*]silolo[2",3"-*d*:"',3'''-*d'*]thiophene (ARSi) is a mutually fused structure hybridized by a BDT unit and two DTS units that share the two thiophene rings with the central BDT core. The ARSi moiety was then copolymerized with naphtho[1,2-*c*:5,6-*c'*]bis[1,2,5]oxadiazole (NO) and 2,1,3-benzoxadiazole (BO) units to form novel alternating copolymers, namely, PSiNO and PSiBO, respectively. Note that the NO acceptor moiety is a symmetrical molecule composed of two oxadiazole units, providing a strong electron withdrawing character and affording better planarity to increase π -conjugation that further enhances close inter- and intramolecular interactions. At the same time, six solubilizing alkyl side-chains for every repeat unit in the ladder-type ARSi can be easily introduced onto the polymer backbone, which could provide a better solution processability of the target polymers. As result, we present a low bandgap copolymer PSiNO with high molecular weight for the first time that performs well in BHJ solar cells, affording a remarkable power conversion efficiency (PCE) of 8.37% along with high open-circuit voltage (V_{oc}) and fill factor (FF) of 0.90 V and 70.2% when blended with PC₇₁BM.

Scheme 1 outlines the chemical structure and synthetic route of two copolymers by Stille cross-coupling reactions under microwave heating conditions. For the donor ARSi unit, the known 4,8-dihexylbenzo[1,2-*b*:4,5-*b'*]dithiophene (**1**)²⁹ with good solubility was selected as the starting material: bromination of **1** with Br₂ gave 2,3,6,7-tetrabromo-4,8-dihexylbenzo[1,2-*b*:4,5-*b'*]dithiophene (**2**); selective Negishi coupling between **2** and (3-bromothiophen-2-yl)-zinc chloride afforded compound **3**; subsequent protection of the free α -positions of **3** by trimethylsilyl (TMS) groups formed compound **4**; lithiation of all four brominated positions of **4** and following ring-closing reaction with dichlorodioctylsilane constructed TMS-modified ARSi (**5**); displacement of TMS groups of **5** by *N*-bromosuccinimide produced compound **6**; stannylation of **6** afforded distannylated monomer **7** ready for polymerization. Inspired by the well-known BO acceptor,⁸ the fused derivative NO acceptor was synthesized from 1,5-dinitronaphthalene-2,6-diamine **8** by a two-step procedure, including oxidative cyclization of **8** with sodium hypochlorite to yield NO's N-oxide **9**, followed by its reduction with triphenylphosphane. Bromination of NO with *N*-bromosuccinimide gave dibromo-derivative DiBr-NO. All products were fully characterized by spectroscopic methods (see Supplementary Information). Furthermore, the chemical structures and the planarity of dibromo-ARSi (**6**) and NO were unambiguously confirmed by single-crystal X-ray diffraction (Fig. S1†). Finally, distannylated-ARSi **7** and DiBr-NO were copolymerized by Stille cross-coupling reactions under microwave heating conditions to obtain the PSiNO copolymer. In this communication, we also synthesized the BO-based analogous PSiBO copolymer for a fair comparison. Crude polymers were purified by Soxhlet extraction with methanol, hexane, and chloroform, respectively. The chloroform solution was concentrated and the product was reprecipitated in methanol to obtain the target copolymers with brown fibrous solids. The number-

average molecular weights (M_n) of the synthesized PSiNO and PSiBO polymers were determined by gel permeation chromatography (GPC) against polystyrene standards in a THF eluent and were found to be as high as 100.4 and 61.8 kDa, with polydispersity indices of 1.5 and 2.8, respectively. High molecular weight is desirable because it will help to improve the film-forming ability and photovoltaic performance. Additionally, to ensure the solubility of the polymer, we adapted the polymer structure by incorporating six flexible aliphatic side-chains into the ARSi unit.

The thermal properties of the polymers were determined by thermogravimetric analysis (TGA) under a nitrogen atmosphere at a heating rate of 10 °C min⁻¹ shown in Fig. S3†. Both polymers are thermally stable with onset decomposition temperatures with 5% weight loss (T_d) at above 380 °C. No obvious thermal transitions were identified in the differential scanning calorimetry (DSC) curves of the second heating and cooling runs, which is attributed to the rigid backbone that limits the chain motion.



Scheme 1 a) Schematic illustration of procedure for the preparation of PSiNO and PSiBO copolymers. b) Synthetic routes of the monomers and polymers. Reagents and conditions: i) Br₂, CHCl₃/CH₃COOH (v/v=2:1), R.T. then reflux. ii) (3-bromothiophen-2-yl)-zinc chloride, Pd(PPh₃)₄, THF, reflux. iii) A) LDA, THF, -60 °C to R.T.; B) TMSCl, -60 °C to R.T. iv) A) *t*-BuLi, THF, -90 °C; B) Si(*n*-Oct)₂Cl₂, -90 °C to R.T. v) NBS, THF, 0 °C. vi) A) *t*-BuLi, THF, -90 °C; B) Me₃SnCl, -90 °C to R.T. vii) 1M NaOH (95% EtOH), 5% NaClO (aq), 0 °C. viii) PPh₃, THF, reflux. ix) NBS, CF₃COOH, H₂SO₄, 0 °C to R.T. x) Pd₂(dba)₃, P(*o*-tol)₃, chlorobenzene.

Fig. 1a shows absorption spectra of two polymers in dilute *o*-DCB solution and as thin films. It can be seen that both polymers exhibit three well-defined absorption bands either in *o*-DCB or in thin films, which imply that these two polymers have order structures both in solution and in thin film. The short-wavelength absorption bands from 400 to 500 nm are assigned to a delocalized excitonic π - π^* transition of the heptacyclic moieties, while the long-wavelength absorption bands with well-resolved vibronic levels in the range of 500 to 900 nm are reasonably ascribed to intramolecular charge transfer (ICT) interactions from the donor to the acceptor unit of the polymer backbone. The 0-0 and 0-1 transitions of PSiBO/PSiNO ICT bands are located at 685/745 nm and 631/682 nm (shoulder), respectively. It has been reported that the greater magnitude of this vibronic peak reveals a more ordered microstructure.³⁰ The sharp ICT bands in their absorption spectra thus indicate that both PSiBO and PSiNO are highly rigid with a coplanar feature of the conjugated structures. Moreover, the intensity ratio for 0-0 versus 0-1 transition

of PSiNO is higher than that of PSiBO. In addition, a second shoulder (0-2 transition) of ICT band of PSiNO appearing at ~600 nm is obscure in PSiBO. For molecules without symmetry constraint, the higher intensity ratio manifests the less change of chromophoric bond distances upon Franck Condon excitation. For D–A polymers, it implies more extensive π -delocalization and hence a higher degree of coplanarity/rigidity. Indirectly, the result leads us to conclude that the acceptor strength of NO (PSiNO) is greater than that of BO (PSiBO). Support of this viewpoint is given by the optical bandgaps (E_g^{opt}) deduced from the absorption onsets of the film spectra, which are in the order of PSiBO (1.70 eV) > PSiNO (1.56 eV).

To gain more insight into the effect of planarization on the molecular structures and electronic properties, theoretical calculations by density functional theory (DFT) model at the B3LYP/6-31G* level were performed on dimers with methyl substituted alkyl chains for simplicity. Both truncated polymers represent excellent planarity through the entirety of the polymer backbone (Fig. 1b). The torsion angles between the D–A repeat units are < 1.3°, implying that the polymer backbone of PSiNO and PSiBO are free of steric hindrance between adjacent D and A units, so that the coplanar conformation can be easily retained in both solution and solid state. The wave functions of the frontier molecular orbital are depicted in Fig. S4†. As can be observed, the electron density in the HOMO wave function is mostly delocalized along the whole polymer backbone, whereas the electron density associated with the LUMO is fairly well-localized at the electron acceptor site. The good wave function delocalization and the coplanarity should facilitate both intra- and intermolecular charge transport.

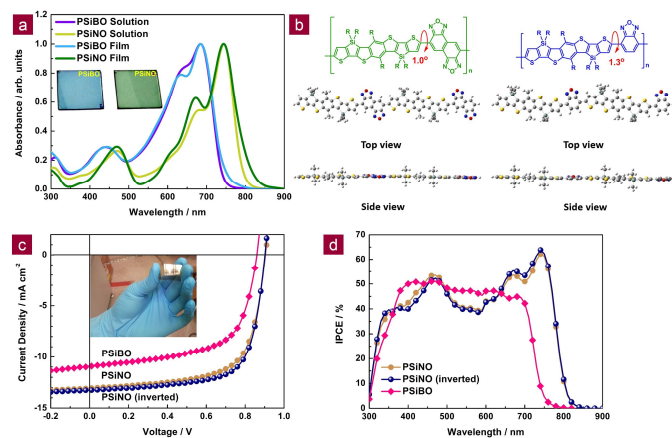


Fig. 1 a) Normalized UV–vis absorption spectra of the target polymers in *o*-DCB solution and as thin films. Inset: Photograph of PSiBO and PSiNO films (from left to right) showing variation in color. b) Minimum energy conformations of dimers of PSiNO (left) and PSiBO (right) with their calculated torsion angles. c) J – V curves of optimized devices based on 1:1.5 PSiNO:PC₇₁BM solar cells with 0.5 vol% DIO and 1:1 PSiBO:PC₇₁BM solar cells with 3 vol% DIO under AM 1.5G solar illumination, and d) corresponding IPCE spectra of optimized 1:1.5 PSiNO:PC₇₁BM and 1:1 PSiBO:PC₇₁BM devices illuminated by monochromatic light. Legend: light brown circles (●) represent the PSiNO conventional device ($V_{\text{oc}} = 0.90$ V, $J_{\text{sc}} = -13.10$ mA cm⁻², FF = 67.4%, and PCE = 7.95%), navy circles (●) represent the PSiNO inverted device ($V_{\text{oc}} = 0.90$ V, $J_{\text{sc}} = -13.25$ mA cm⁻², FF = 70.2%, and PCE = 8.37%) and pink diamonds (◆) represent the PSiBO conventional device ($V_{\text{oc}} = 0.86$ V, $J_{\text{sc}} = -10.93$ mA cm⁻², FF = 62.3%, and PCE = 5.86%).

Cyclic voltammetry (CV) was then employed to measure the onset red/ox potentials of the polymers (Fig. S5†). The HOMO/LUMO energies for PSiNO and PSiBO are -5.50/-3.73 eV and -5.46/-3.55 eV, respectively. The silole unit is known to possess certain extent of electron-accepting ability, which in turn lowers the HOMO/LUMO energy levels of PSiNO and PSiBO polymers.³¹ Compared to PSiNO, PSiBO shows higher-lying HOMO/LUMO energy levels, inferring weaker electron-withdrawing ability of the BO fragment than that of the NO unit (*vide supra*). Since V_{oc} of BHJ PSCs correlates closely with the difference between the LUMO energy level of the fullerene and HOMO energy level of the donor polymer, a larger V_{oc} for NO-based PSCs is anticipated. The LUMO energy levels of these two polymers are located at -3.55 to -3.73 eV, providing sufficient driving force for charge separation and electron transfer without too much energy loss.

Hole mobility of two polymers (PSiNO and PSiBO) was measured by space charge limit current (SCLC) method.³² PSiNO demonstrates a relatively high hole mobility of 1.2×10^{-3} cm² V⁻¹ s⁻¹, which is around three times higher than that of PSiBO (4.3×10^{-4} cm² V⁻¹ s⁻¹) (see Fig. S6†). This variation in device behavior can be attributed to the change of the coplanarity in the polymer backbone by the introduction of different acceptors, and we can conclude that the fused NO acceptor enhances the intrachain mobility because of more extended π -conjugation and less steric hindrance as compared to the nonfused BO acceptor. This facilitates carrier collection efficiency and hence partly accounts for the higher fill factor (FF) and short-circuit current density (J_{sc}) values for PSiNO based devices elaborated below.

To characterize the photovoltaic properties for PSiNO and PSiBO, conventional BHJ PSCs using ITO/PEDOT:PSS (40 nm)/polymer:PC₇₁BM (90–115 nm)/poly[(9,9-dioctyl-2,7-fluorene)-alt-(9,9-bis(3'-(*N,N*-dimethylamino)propyl)-2,7-fluorene)] (PFN) (5 nm)/Ca (20nm)/Al (100nm) device configuration were prepared and examined under simulated 100 mW cm⁻² AM 1.5G illumination. The incorporation of thin PFN cathode interlayer can construct interfacial dipole, which could result in the reduced electron injection barrier and enhanced built-in potential across the device.¹⁴ The optimized polymer to PC₇₁BM ratios of PSiNO and PSiBO used to form the active layers of the PSCs were 1:1.5 and 1:1, respectively. The polymer active layers of PSiNO and PSiBO were spin-coated from *o*-DCB solutions with 0.5% and 3% (v/v) 1,8-diiodooctane (DIO) additives,³³ respectively. We optimized the thickness of the active layers and found that 90–115 nm was the best thickness for all devices. The J – V curves and incident photon-to-current efficiencies (IPCE) of solar cells are presented in parts c and d of Fig. 1. The detailed device performances are summarized in Table 1. In the optimized 1:1.5 PSiNO:PC₇₁BM device without further thermal annealing treatment, the V_{oc} reaches up to 0.90 V, with a J_{sc} of 13.10 mA cm⁻² and a FF of 67.4%, offering a high PCE of 7.95%. Conversely, device based on optimized 1:1 PSiBO:PC₇₁BM acquires a moderate PCE of 5.86%, with a V_{oc} of 0.86 V, a J_{sc} of 10.93 mA cm⁻² and a FF of 62.3%. Further increase of the fullerene ratio yielded negative effect in both J_{sc} and FF, which resulted in a decreased PCE. As expected from the low-lying HOMO energy levels of the polymers, the trend in V_{oc} agrees well with the electrochemical potentials. Encouragingly, inverted device configuration of ITO/ZnO (40 nm)/PFN (5 nm)/PSiNO:PC₇₁BM/MoO₃ (8 nm)/Ag (100 nm) leads to a superior device performance compared to the conventional device architecture, showing a V_{oc} of 0.90 V, a J_{sc} of 13.25 mA cm⁻² and a FF of 70.2%, delivering an exceptional PCE of 8.37%, owing to the improved J_{sc} and FF. We recognized that both J_{sc} and FF of PSiNO based devices

were much higher than those of PSiBO based devices, which could be attributed to various factors: the absorption strength of the active layer, optimal morphology with proper domain size of the active layer and higher charge carrier mobility that can promote the exciton separation, charge transport, and enhanced charge collection efficiency, resulting in simultaneously increased J_{sc} and FF.³⁴ To verify the accuracy of the photo J - V measurements, the corresponding IPCE spectra of the devices elaborated above were measured under illumination of monochromatic light shown in Fig. 1d. Compared to the absorption spectra of pristine polymers, the substantially broadened IPCE responses in the visible region can be attributed to both the intrinsic absorptions of the polymers and PC₇₁BM. The IPCE spectra accord well with the absorption spectra of the blends (Fig. S8†), establishing a close correlation with the photocurrents. The integrated J_{sc} values from the IPCE spectra are 12.68, 12.73 and 10.40 mA cm⁻² for conventional PSiNO, inverted PSiNO and conventional PSiBO devices, respectively. The J_{sc} values calculated from integration of the IPCE spectra are within 5% error, which conform well to those obtained from the J - V measurements, supporting the reliability of the photovoltaic measurement.

To further shed light on the difference in the molecular packing and nanostructural order, synchrotron grazing incidence wide-angle X-ray scattering (GIWAXS) analysis was performed to examine the neat polymer films and the optimized 1:1.5 PSiNO:PC₇₁BM blend film. In Fig. 2a and b, both polymers show arc and anisotropic ring scattering patterns. The Bragg scattering peaks of (100) appear relatively strong in intensity at $q = 0.375 \text{ \AA}^{-1}$ with an interlayer d_{100} spacing of 16.8 Å and $q = 0.351 \text{ \AA}^{-1}$ and an interlayer d_{100} spacing of 17.9 Å for PSiNO and PSiBO, respectively, corresponding to the periodic lamellae of polymer backbones. The weak diffraction peaks at $q = 0.753 \text{ \AA}^{-1}$ and 0.703 \AA^{-1} for PSiNO and PSiBO represent the second-order (200) reflections of lamellae (d_{200} spacing = 8.34 Å and 8.94 Å). Furthermore, the stronger intensity of the (100) reflection in the out-of-plane scattering profile than in the in-plane scattering profile indicates that the lamellar packing of both polymers preferentially stacked out of the film plane, though with some randomness. The results are attributable to the introduction of six flexible aliphatic side-chains into the ARSi unit, resulting in the misorientation of the polymer lamellae.³⁵ Nevertheless, this high degree of lamellar stacking can be related to the planarity and rigidity of the polymer backbone, which enhances intramolecular charge transport as well as intermolecular charge transport parallel to the ITO substrate. It is also worth mentioning that the d_{100} spacing of PSiNO is different from that of PSiBO by 1.1 Å, indicating that the NO unit offers more space to promote the close packing of alkyl side-chains interdigitating and/or tilting out of the polymer backbone plane in the solid state (Fig. S9†). Therefore, PSiNO polymer chains are stacked more tightly than PSiBO polymer chains. The net result is to affect intermolecular interactions and promote molecular packing. Additionally, a smaller d spacing for PSiNO may facilitate intermolecular charge transfer in high performance PSCs. The (010) reflections were almost undetectable, indicating a poor π - π stacking of polymer backbones owing to the out-of-plane side-chains that inhibit the order packing of polymer backbones. In Fig. 2c, the $q = 1.4 \text{ \AA}^{-1}$ halo is typically attributable to amorphous scattering from the PC₇₁BM aggregation within the blend, indicating random orientation with respect to the film substrate. Again, no clear π - π stacking reflection peak can be observed for the blend, suggesting low crystallinities in the polymer blend. However, the lamellar packing is still visible in the blends, indicating that the PSiNO is able to maintain the same molecule arrangement when blended with fullerene. Therefore, the high hole mobility of the polymers thus not results from the hopping of holes through an ordinary order π - π

stacking route.³⁶⁻³⁸ The novelty of this new polymer therefore lies in its great rigidity and planarity of the backbone so that the chain folding is inhibited and polymer chains should be rather extended. Such extended chains allow charge carriers to directly transport and/or percolation through the low-resistant polymer backbones, leading to the high carrier mobility.

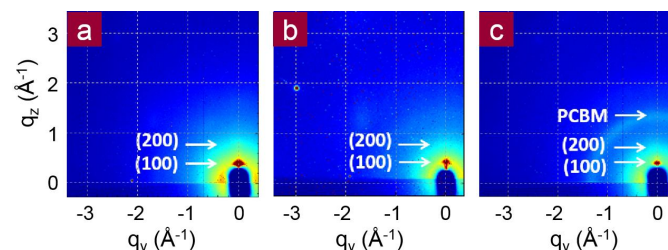


Fig. 2 Two-dimensional grazing incidence wide-angle X-ray scattering (GIWAXS) patterns of a) PSiNO, b) PSiBO neat films and c) PSiNO:PC₇₁BM (1:1.5) blend film.

To gain deeper insight into the effect of nanoscale morphology of the photoactive layers on PSCs, the morphological structures of both optimized blend films were analyzed by tapping-mode atomic force microscopy (TM-AFM) measurements.³⁹ As a result, PSiNO and PSiBO blends displayed very different morphologies. Nanoscale fibril features are clearly manifested from the PSiNO:PC₇₁BM blend with a root mean square (RMS) roughness of 4.2 nm. The well phase separation is consistent with the more pronounced intermolecular stacking, as evidenced by the GIWAXS analysis (Fig. 3a). In stark contrast, PSiBO:PC₇₁BM blend exhibited unevenly aggregated polymer and PC₇₁BM domains with a RMS roughness of 5.4 nm (Fig. 3b). This adverse morphology may limit the exciton dissociation probability, resulting in exciton loss, geminate charge recombination, and poor charge mobility.^{11,39} The well-ordered domains within the matrix, together with the high hole mobility of PSiNO, are likely to enable efficient charge separation and transport, which help to rationalize the good performance of PSCs.

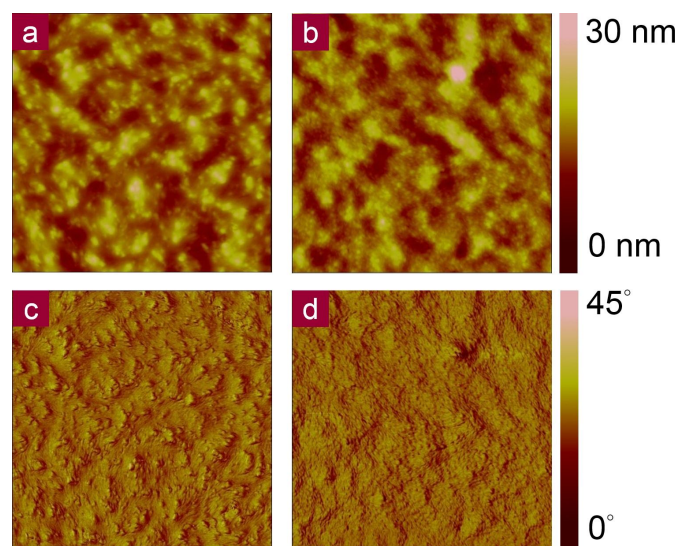


Fig. 3 Morphology characterization of TM-AFM topography images (upper row) and phase images (lower row) of 1:1.5 PSiNO:PC₇₁BM blend films with 0.5 vol% DIO (panels a and c) and 1:1 PSiBO:PC₇₁BM blend films with 3 vol% DIO (panels b and d). The imaging size is 3 μm \times 3 μm for each panel.

Table 1 Photovoltaic parameters of optimized solar cells.

Polymer	Polymer: PC ₇₁ BM	V _{oc} (V)	J _{sc} (mA cm ⁻²)	FF (%)	PCE ^{a)} (%)
PSiNO	1:1	0.90	12.88	62.1	7.20 (6.94)
PSiNO	1:1.5	0.90	13.10	67.4	7.95 (7.76)
PSiNO ^{b)}	1:1.5	0.90	13.25	70.2	8.37 (8.08)
PSiNO	1:2	0.88	11.65	58.3	5.98 (5.70)
PSiBO	1:1	0.86	10.93	62.3	5.86 (5.62)
PSiBO	1:1.5	0.86	10.38	60.1	5.37 (5.10)
PSiBO	1:2	0.84	9.18	55.4	4.27 (3.95)

^{a)} Average PCE of 10 optimized devices in parentheses. ^{b)} Inverted device configuration of ITO/ZnO/PFN/PSiNO:PC₇₁BM/MoO₃/Ag.

In conclusion, two kinds of highly rigidified and coplanar low bandgap ladder-type copolymers of PSiNO and PSiBO upon naphthobisoxadiazole (NO) and benzoxadiazole (BO) with silicon-bridged heptacyclic arene (ARSi) are designed and synthesized. Both polymers show relatively low-lying HOMO energy levels that consequently result in high open-circuit voltage of the solar cell devices. Unambiguously, both electron-donor ARSi and acceptor NO in this study are brand-new in both synthetic chemistry and solar cell applications. On the one hand, the design strategy for ARSi is to provide a three-in-one functionality: planarity, rigidity and charge transport efficiency. On the other hand, functionalizing the strong electron-withdrawing ability of NO moiety leads to stronger inter- and intra-chain interactions, higher charge carrier mobility as well as extension of the absorption spectra towards near IR region, along with lowering the HOMO, LUMO energy levels and optical bandgap. With an inverted device structure, the maximum solar efficiency upon PSiNO:PC₇₁BM reaches 8.37% along with an open-circuit voltage of 0.90 V, a short-circuit current density of 13.25 mA cm⁻² and a fill factor of 70.2% without thermal annealing, demonstrating that ARSi and NO moieties are a promising electron-donor/acceptor combination to build up high-performance photovoltaics. More importantly, the high starting point acquired in this device architecture, together with the low-ordering polymer framework, makes possible further improvement to reach records by integrating more efficient device architecture innovation, such as ternary blends upon adding small organic dyes, plasmonic, or microcavity architectures.

Acknowledgements

The devices fabrication was carried out in Advanced Laboratory of Accommodation and Research for Organic Photovoltaics, Ministry of Science and Technology of Taiwan. This work was also financially supported by the Ministry of Science and Technology of Taiwan.

Notes and references

^{a)} Department of Chemistry

Center of Emerging Material and Advanced Devices

National Taiwan University, Taipei 106, Taiwan.

E-mail: kenwong@ntu.edu.tw, chop@ntu.edu.tw

^{b)} Research Center for New Generation Photovoltaics

Graduate Institute of Energy Engineering

National Central University, Zhongli, 320, Taiwan.

E-mail: austinchen@ncu.edu.tw

^{c)} Department of Chemical Engineering

National Taiwan University, Taipei 106, Taiwan.

^{d)} Institute of Polymer Science and Engineering

National Taiwan University, Taipei 106, Taiwan.

† Electronic supplementary information (ESI) available. See

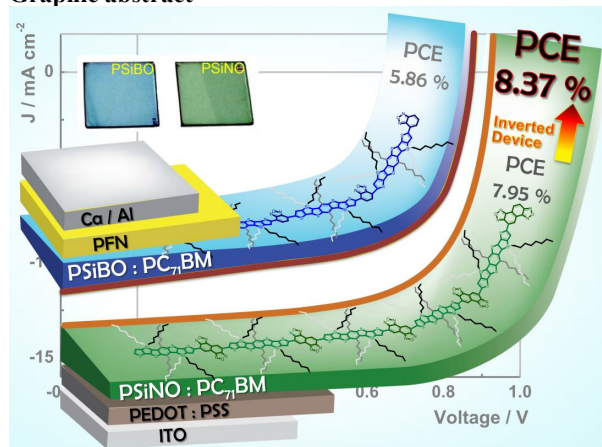
DOI: 10.1039/c000000x/

‡ These authors contributed equally to this work.

- B. Kippelen and J.-L. Brédas, *Energy Environ. Sci.*, 2009, **2**, 251.
- S. C. Price, A. C. Stuart, L. Yang, H. Zhou and W. You, *J. Am. Chem. Soc.*, 2011, **133**, 4625.
- C. E. Small, S. Chen, J. Subbiah, C. M. Amb, S.-W. Tsang, T.-H. Lai, J. R. Reynolds and F. So, *Nat. Photonics*, 2012, **6**, 115.
- H.-C. Chen, Y.-H. Chen, C.-C. Liu, Y.-C. Chien, S.-W. Chou and P.-T. Chou, *Chem. Mater.*, 2012, **24**, 4766.
- X. Guo, F. Liu, S. Zhang, L. Huo, T. P. Russell and J. Hou, *Adv. Mater.*, 2013, **25**, 4944.
- I. Osaka, T. Kakara, N. Takemura, T. Koganezawa and K. Takimiya, *J. Am. Chem. Soc.*, 2013, **135**, 8834.
- H.-C. Chen, Y.-H. Chen, C.-H. Liu, Y.-H. Hsu, Y.-C. Chien, W.-T. Chuang, C.-Y. Cheng, C.-L. Liu, S.-W. Chou, S.-H. Tung and P.-T. Chou, *Polym. Chem.*, 2013, **4**, 3411.
- X. Wang, P. Jiang, Y. Chen, H. Luo, Z. Zhang, H. Wang, X. Li, G. Yu and Y. Li, *Macromolecules*, 2013, **46**, 4805.
- S. B. Darling and F. You, *RSC Adv.*, 2013, **3**, 17633.
- C. Cui, W.-Y. Wong and Y. Li, *Energy Environ. Sci.*, 2014, **7**, 2276.
- H.-C. Chen, S.-W. Chou, W.-H. Tseng, I.-W. P. Chen, C.-C. Liu, C. Liu, C.-L. Liu, C.-h. Chen, C.-I. Wu and P.-T. Chou, *Adv. Funct. Mater.*, 2012, **22**, 3975.
- X. Li, W. C. H. Choy, L. Huo, F. Xie, W. E. I. Sha, B. Ding, X. Guo, Y. Li, J. Hou, J. You and Y. Yang, *Adv. Mater.*, 2012, **24**, 3046.
- Z.-G. Zhang, B. Qi, Z. Jin, D. Chi, Z. Qi, Y. Li and J. Wang, *Energy Environ. Sci.*, 2014, **7**, 1966.
- Z. He, C. Zhong, X. Huang, W.-Y. Wong, H. Wu, L. Chen, S. Su and Y. Cao, *Adv. Mater.*, 2011, **23**, 4636.
- C.-Z. Li, C.-Y. Chang, Y. Zang, H.-X. Ju, C.-C. Chueh, P.-W. Liang, N. Cho, D. S. Ginger and A. K.-Y. Jen, *Adv. Mater.*, 2014, **26**, 6262.
- W. Cao and J. Xue, *Energy Environ. Sci.*, 2014, **7**, 2123.
- Z. He, C. Zhong, S. Su, M. Xu, H. Wu and Y. Cao, *Nat. Photonics*, 2012, **6**, 591.
- Y. Sun, C. J. Takacs, S. R. Cowan, J. H. Seo, X. Gong, A. Roy and A. J. Heeger, *Adv. Mater.*, 2011, **23**, 2226.
- Z. Xu, L.-M. Chen, G. Yang, C.-H. Huang, J. Hou, Y. Wu, G. Li, C.-S. Hsu and Y. Yang, *Adv. Funct. Mater.*, 2009, **19**, 1227.
- J. H. Seo, A. Gutacker, Y. Sun, H. Wu, F. Huang, Y. Cao, U. Scherf, A. J. Heeger and G. C. Bazan, *J. Am. Chem. Soc.*, 2011, **133**, 8416.
- A. Kumar, G. Lakhwani, E. Elmaleh, W. T. S. Huck, A. Rao, N. C. Greenham and R. H. Friend, *Energy Environ. Sci.*, 2014, **7**, 2227.
- J. E. Anthony, *Chem. Rev.*, 2006, **106**, 5028.
- C.-Y. Chang, Y.-J. Cheng, S.-H. Hung, J.-S. Wu, W.-S. Kao, C.-H. Lee and C.-S. Hsu, *Adv. Mater.*, 2012, **24**, 549.
- Y.-X. Xu, C.-C. Chueh, H.-L. Yip, F.-Z. Ding, Y.-X. Li, C.-Z. Li, X. Li, W.-C. Chen and A. K. -Y. Jen, *Adv. Mater.*, 2012, **24**, 6356.

- 25 J.-S. Wu, S.-W. Cheng, Y.-J. Cheng and C.-S. Hsu, *Chem. Soc. Rev.*, 2014, DOI: 10.1039/C4CS00250D.
- 26 H.-Y. Chen, J. Hou, A. E. Hayden, H. Yang, K. N. Houk and Y. Yang, *Adv. Mater.*, 2010, **22**, 371.
- 27 M. C. Scharber, M. Koppe, J. Gao, F. Cordella, M. A. Loi, P. Denk, M. Morana, H.-J. Egelhaaf, K. Forberich, G. Dennler, R. Gaudiana, D. Waller, Z. Zhu, X. Shi and C. J. Brabec, *Adv. Mater.*, 2010, **22**, 367.
- 28 Y.-L. Chen, C.-Y. Chang, Y.-J. Cheng and C.-S. Hsu, *Chem. Mater.*, 2012, **24**, 4766.
- 29 H. Pan, Y. Li, Y. Wu, P. Liu, B. S. Ong, S. Zhu and G. Xu, *J. Am. Chem. Soc.*, 2007, **129**, 4112.
- 30 R. C. Coffin, J. Peet, J. Rogers and G. C. Bazan, *Nat. Chem.*, 2009, **1**, 657.
- 31 B. C. Schroeder, R. S. Ashraf, S. Thomas, A. J. P. White, L. Biniak, C. B. Nielsen, W. Zhang, Z. Huang, P. S. Tuladhar, S. E. Watkins, T. D. Anthopoulos, J. R. Durrant and I. McCulloch, *Chem. Commun.*, 2012, **48**, 7699.
- 32 V. D. Mihaileti, H. Xie, B. de Boer, L. J. A. Koster and P. W. M. Blom, *Adv. Funct. Mater.*, 2006, **16**, 699.
- 33 H.-C. Liao, C.-C. Ho, C.-Y. Chang, M.-H. Jao, S. B. Darling and W.-F. Su, *Mater. Today*, 2013, **9**, 326.
- 34 Y. Liang, Y. Wu, D. Feng, S.-T. Tsai, H.-J. Son, G. Li and L. Yu, *J. Am. Chem. Soc.*, 2009, **131**, 56.
- 35 I. Osaka, R. Zhang, J. Liu, D.-M. Smilgies, T. Kowalewski and R. D. McCullough, *Chem. Mater.*, 2010, **22**, 4191.
- 36 H. Bronstein, D. S. Leem, R. Hamilton, P. Woebkenberg, S. King, W. Zhang, R. S. Ashraf, M. Heeney, T. D. Anthopoulos, J. de Mello and I. McCulloch, *Macromolecules*, 2011, **44**, 6649.
- 37 H. Bronstein, Z. Chen, R. S. Ashraf, W. Zhang, J. Du, J. R. Durrant, P. S. Tuladhar, K. Song, S. E. Watkins, Y. Geerts, M. M. Wienk, R. A. J. Janssen, T. Anthopoulos, H. Sirringhaus, M. Heeney and I. McCulloch, *J. Am. Chem. Soc.*, 2011, **133**, 3272.
- 38 X. Zhang, L. J. Richter, D. M. DeLongchamp, R. J. Kline, M. R. Hammond, I. McCulloch, M. Heeney, R. S. Ashraf, J. N. Smith, T. D. Anthopoulos, B. Schroeder, Y. H. Geerts, D. A. Fischer and M. F. Toney, *J. Am. Chem. Soc.*, 2011, **133**, 15073.
- 39 W. Chen, M. P. Nikiforov and S. B. Darling, *Energy Environ. Sci.*, 2012, **5**, 8045.

Graphic abstract



We present a silole-containing ladder-type copolymer PSiNO with high molecular weight affording a remarkable PCE of 8.37%.

Broader context box

The donor–acceptor (D–A) copolymers based on benzo[1,2-*b*:4,5-*b'*]dithiophene (BDT) and dithieno[3,2-*b*:2',3'-*d*]silole (DTS) show broad absorption, relatively low-lying HOMO energy level and high hole mobility, indicating that BDT and DTS have emerged as attractive building blocks for highly efficient conjugated polymers. These results inspire us to hybridize BDT/DTS units into mutually fused structures to promote planarity and charge transport efficiency, which could provide an opportunity to tune the optoelectronic properties and expect to improve the photovoltaic performance. In this study, we report a straightforward synthetic methodology to prepare a series of brand-new, high rigidified and coplanar low bandgap ladder-type D–A alternating copolymers combining a seven-ring heteroacene ARSi as the donor unit, and a dually-fused ring NO or nonfused ring BO as acceptor moieties. Both polymers show relatively low-lying HOMO energy levels that consequently lead to high open-circuit voltage of the solar cell devices. Functionalizing the strong electron-withdrawing ability of NO moiety leads to the enhancement of absorption intensity as well as extension of the absorption spectra towards near IR region, along with lowering the HOMO, LUMO energy levels and optical bandgap. Most significantly, BHJ inverted device upon PSiNO:PC₇₁BM blend achieves an impressively high PCE of 8.37% without thermal annealing, demonstrating PSiNO can be a promising semiconducting polymer for high-performance photovoltaics.

Supplementary Information

A promising combination of brand-new silole-containing ladder-type heptacyclic arene and naphthobisoxadiazole moieties for highly efficient polymer solar cells

Zhiyun Zhang,^{‡a} Francis Lin,^{‡a} Hsieh-Chih Chen,^{*a,b} Hung-Chin Wu,^c Chin-Lung Chung,^a Chien Lu,^c Shih-Hung Liu,^a Shih-Huang Tung,^d Wen-Chang Chen,^{cd} Ken-Tsung Wong,^{*a} and Pi-Tai Chou^{*a}

^a Department of Chemistry
Center of Emerging Material and Advanced Devices
National Taiwan University, Taipei 106, Taiwan.
E-mail: kenwong@ntu.edu.tw, chop@ntu.edu.tw

^b Research Center for New Generation Photovoltaics
Graduate Institute of Energy Engineering
National Central University, Jhongli, 320, Taiwan.
E-mail: austinchen@ncu.edu.tw

^c Department of Chemical Engineering
National Taiwan University, Taipei 106, Taiwan.

^d Institute of Polymer Science and Engineering
National Taiwan University, Taipei 106, Taiwan.

Experimental Section

Measurement and Characterization: All NMR spectra were obtained on a Varian Mercury 400 in deuterated chloroform solution with 0.003%TMS as internal reference. Mass spectra were obtained on a FINNIGAN LCQ mass spectrometer. Chemical shift (δ) were reported in parts per million (ppm), and coupling constant (J) were recorded in Hertz (Hz). Molecular weight and molecular weight distribution were analyzed by a Waters GPC (Breeze system) using tetrahydrofuran (THF) as an eluent at 35 °C. The apparatus was equipped with two Waters Styragel columns (HR3 and HR4E), a refractive index detector (Waters 2414), and a dual-wavelength absorbance detector (Waters 2487). Polystyrene standards (Waters) were used for calibration. The polymer film was coated on ITO sheets by solvent casting. Cyclic voltammetry (CV) was conducted on an Autolab PGSTAT 30 Electrochemical Workstation with Ag, Ag/Ag⁺, Pt wire as working electrode, reference electrode, and counter electrode,

respectively, in a solution of 0.1 M tetrabutylammonium perchlorate (Bu_4NCl_6) in deoxygenated acetonitrile (CH_3CN) at a scan rate of 50 mV s^{-1} . The potential of the polymer was corrected in the standard of Fc/Fc^+ in CH_3CN (0.45 V vs. Ag/Ag^+ electrode). Thermogravimetric analysis (TGA) and differential scanning calorimetry (DSC) measurements were performed under a nitrogen atmosphere at heating rates of 10 and $5 \text{ }^\circ\text{C min}^{-1}$ using a TA Instruments (TGA-951 and DSC-910S, respectively). Tapping mode atom force microscopy (TM-AFM) images were taken on a NanoScope IIIa controller (Veeco Metrology Group/Digital Instruments, Santa Barbara, CA), using built-in software (version V6.13R1) to capture images. Grazing incidence wide-angle X-ray scattering (GIWAXS) measurements were conducted at the BL23A1 endstation of the National Synchrotron Radiation Research Center (NSRRC), Taiwan. The thin films for characterization were deposited on a $1 \text{ cm} \times 2 \text{ cm}$ silicon wafer. A monochromatic beam of wavelength $\lambda = 0.826 \text{ \AA}$ (15 keV) was used and the incident angle was 0.2° . The scattering patterns were collected on a CMOS flat panel X-ray detector C9728DK ($52.8 \text{ mm} \times 52.8 \text{ mm}$). The scattering intensity profiles were extracted from the 2D patterns and reported as the plots of the scattering intensity I vs. the scattering vector q , where $q = (4\pi/\lambda) \sin(\theta/2)$ and θ is the scattering angle. The absorption spectra were obtained on a Hitachi U-4100 spectrophotometer. Hole-only devices were fabricated according to a similar method described in the literature,^[1] using a diode configuration of ITO/PEDOT:PSS/polymer/Pd (50 nm). The SCLC current was measured under dark conditions using a Keithley 2400 Source Meter.

Solar Cell Device Fabrication and Characterization: The conventional PSCs were fabricated with the device structure of ITO/PEDOT:PSS (40 nm)/polymer:PC₇₁BM (90-115 nm)/poly[(9,9-dioctyl-2,7-fluorene)-alt-(9,9-bis(3'-(*N,N*-dimethylamino)propyl)-2,7-fluorene)] (PFN) (5 nm)/Ca (20nm)/Al (100nm). Prior to use, patterned ITO-coated glass substrates ($15 \text{ } \Omega/\text{square}$) were successively cleaned by ultrasonication in 1% neutral detergent in water, then

deionized water, followed by acetone and finally isopropanol for 10 min each and subsequently dried under a stream of dry nitrogen. The substrates were then underwent oxygen plasma treatment for 20 min prior to the deposition of a ~40-nm-thick layer of PEDOT:PSS, as verified by a Filmetrics Model F10-RT-UV system. Deposition of the PEDOT:PSS layer was followed by baking at 150 °C for 15 min in air and then transferred into an inert N₂-filled glove box (< 0.1 ppm O₂ and H₂O) for subsequent procedures. Blend solutions were prepared by dissolving the target polymer (PSiNO or PSiBO) and PC₇₁BM (purchased from Nano-C) in *o*-DCB solution in blend ratios of 1:1, 1:1.5 and 1:2 with a polymer concentration of 10 mg mL⁻¹ and were heated to 100 °C and stirred 8 h for complete dissolution. Then the blend solution was spin-casted after adding 0.5% and 3% (v/v) DIO for PSiNO and PSiBO-based systems. The wet film was slowly dried in a covered Petri dish for 30 min in the glove box. Afterwards, methanol was dropped onto the active layer with a spin-casting rate at 2000 rpm for 60 s, and subsequently PFN interfacial layer was spin-casted onto the active layer according to a similar method described in the literature.^[2] The coated substrates were then transferred to a thermal evaporator and evacuated to $\leq 5 \times 10^{-6}$ Torr before a 20-nm-thick calcium layer followed by a 100-nm aluminium electrode layer were deposited. The effective area of one cell was 0.04 cm². The fabricated device was encapsulated in a nitrogen-filled glove box with UV epoxy and cover glass. The inverted PSCs were fabricated with the configuration of ITO/ZnO (40 nm)/PFN (5 nm)/PSiNO:PC₇₁BM (~110 nm)/MoO₃ (8 nm)/Ag (100 nm). Molybdenum oxide was thermally deposited on top of the active layer with an evaporation rate of 0.1 Å s⁻¹ under a vacuum $\leq 5 \times 10^{-6}$ Torr. Ultimately, 100 nm silver film was deposited on top of the molybdenum oxide layer through a shade mask. The *J-V* curves were measured with a Newport-Oriel (Sol3A Class AAA Solar Simulators) AM 1.5G light source operating at 100 mW cm⁻², and independently cross-checked using a 300 W AM 1.5G source operating at 100 mW cm⁻² for verification. The light intensity was determined by a monosilicon detector (with

KG-5 visible color filter) calibrated by the National Renewable Energy Laboratory (NREL) to minimize spectral mismatch. An IPCE (QE10) characterization platform supplied by PV Measurement, Inc. was used for data acquisition. All IPCE spectra were recorded using a lock-in technique at a chopping frequency of 100 Hz.

Synthetic Procedures: All chemicals and reagents were used as received from commercial sources without further purification. Solvents for chemical synthesis were purified by distillation. All chemical reactions were carried out under an argon or nitrogen atmosphere.

*Synthesis of 2,3,6,7-tetrabromo-4,8-dihexylbenzo[1,2-*b*:4,5-*b'*]dithiophene (2):* 4,8-Dihexylbenzo[1,2-*b*:4,5-*b'*]dithiophene (**1**, 8.61 g, 24 mmol) was dissolved in a mixed solvent of chloroform (240 mL) and acetic acid (120 mL). Bromine (2.47 mL, 48 mmol) was added dropwise into the reaction mixture through an addition funnel under absence of light, and then stirred for 1h at room temperature. More bromine (3.71 mL, 72 mmol) was then added, and the reactant was heated to 80 °C for overnight after the addition. After cooling to room temperature, the reactant was poured into a mixture of ice and saturated NaOH aqueous solution, followed by extraction with water and CH₂Cl₂. The combined extracts was washed with brine, dried over anhydrous MgSO₄, and then filtrated. The solvent was removed by rotary evaporation, and the crude product was washed with methanol to afford **2** as a pale yellow solid (13.53 g, 84 %). ¹H NMR (CDCl₃, 400 MHz) δ 3.39 (t, *J* = 8.4 Hz, 4H), 1.76-1.68 (m, 4H), 1.53-1.47 (m, 4H), 1.37-1.34 (m, 8H), 0.91 (t, *J* = 6.8 Hz, 6H); ¹³C NMR (CDCl₃, 100 MHz) δ 138.9, 130.0, 129.2, 116.8, 109.1, 31.6, 31.2, 31.0, 29.6, 14.2; HRMS (*m/z*, FAB⁺) Calcd for C₂₂H₂₆⁷⁹Br₄S₂ 669.8209, found 669.8207; calcd for C₂₂H₂₆⁷⁹Br₃⁸¹BrS₂ 671.8189, found 671.8192; calcd for C₂₂H₂₆⁷⁹Br₂⁸¹Br₂S₂ 673.8168, found 673.8164; calcd for C₂₂H₂₆⁷⁹Br⁸¹Br₃S₂ 675.8148, found 675.8157; calcd for C₂₂H₂₆⁸¹Br₄S₂ 677.8128, found 677.8126.

Synthesis of 3,7-dibromo-2,6-bis(3-bromothiophen-2-yl)4,8-dihexylbenzo[1,2-b:4,5-b']dithiophene (3): To a flame-dried three neck flask was added 2,3-dibromothiophene (14.52 g, 60 mmol) and anhydrous ether (60 mL) under argon atmosphere. The solution was cooled to -78 °C, before *n*-BuLi (1.6 M in hexane, 37.50 mL, 60 mmol) was added dropwise. After the addition was completed, the reactant was stirred at -78 °C for 1h, and an 0.5 M THF solution of ZnCl₂ (120 mL, 60 mmol) was added quickly. The reactant was then stirred at 0 °C for 1h, and transferred through cannula into a two neck flask containing a solution of **2** (13.48 g, 20 mmol) and Pd(PPh₃)₄ (1.85 g, 1.6 mmol) in anhydrous THF (120 mL). After heated to reflux for 4 days, the reactant was cooled to room temperature and quenched with saturated NH₄Cl aqueous solution (200 mL), followed by extraction with water and ether. The combined extracts was washed with brine, dried over anhydrous MgSO₄, and then filtrated. The solvent was removed by rotary evaporation, and the crude product was purified by column chromatography on silica gel with hexane as eluent to afford **3** as a bright yellow solid (8.65 g, 52 %). ¹H NMR (CDCl₃, 400 MHz) δ 7.50 (d, *J* = 5.6 Hz, 2H), 7.14 (d, *J* = 5.6 Hz, 2H), 3.60 (t, *J* = 8.4 Hz, 4H), 1.90-1.82 (m, 4H), 1.59-1.52 (m, 4H), 1.43-1.33 (m, 8H), 0.91 (t, *J* = 6.8 Hz, 6H); ¹³C NMR (CDCl₃, 100 MHz) δ 139.3, 130.9, 130.8, 130.7, 129.9, 128.2, 113.5, 108.6, 31.6, 31.4, 31.0, 29.7, 22.8, 14.2; HRMS (*m/z*, ESI, [M+Na]⁺) Calcd for C₃₀H₃₀⁷⁹Br₄S₄Na 856.7862, found 856.7847; calcd for C₃₀H₃₀⁷⁹Br₃⁸¹BrS₄Na 858.7841, found 858.7828; calcd for C₃₀H₃₀⁷⁹Br₂⁸¹Br₂S₄Na 860.7821, found 860.7814; calcd for C₃₀H₃₀⁷⁹Br⁸¹Br₃S₄Na 862.7800, found 862.7787; calcd for C₃₀H₃₀⁸¹Br₄S₄Na 864.7780, found 864.7771.

Synthesis of 3,7-dibromo-2,6-bis(4-bromo-2-trimethylsilylthiophen-5-yl)4,8-dihexylbenzo[1,2-b:4,5-b']dithiophene (4): To a solution of diisopropylamine (2.99 mL, 21.3 mmol) in anhydrous THF (10.65 mL) was added *n*-BuLi (1.6 M in hexane, 13.31 mL, 21.3 mmol) dropwise at 0 °C under argon atmosphere. After being stirred at 0 °C for 30 minutes, the ice

bath was removed and the reactant was warmed to room temperature followed by stirring for an additional 30 minutes. The freshly made lithium diisopropylamide solution was then transferred into an addition funnel which was attached onto a two neck bottle containing a solution of **3** (6.88 g, 8.20 mmol) in anhydrous THF (246 mL) before it was added dropwise into the solution at -60 °C. The reactant was stirred at same temperature for 30 minutes, 30 minutes at 0 °C, and then cooled down to -60 °C again before the addition of trimethylchlorosilane (3.12 mL, 24.6 mmol). After the addition, the reactant was stirred overnight and slowly warmed to room temperature, quenched with water and extracted with ether. The combined extracts was washed with brine, dried over anhydrous MgSO₄, and then filtrated. The solvent was removed by rotary evaporation, and the crude product was purified by column chromatography on silica gel with hexane as eluent to afford **4** as a bright yellow solid (7.03 g, 89 %). ¹H NMR (CDCl₃, 400 MHz) δ 7.21 (s, 2H), 3.59 (t, *J* = 8.4 Hz, 4H), 1.88-1.84 (m, 4H), 1.56-1.53 (m, 4H), 1.41-1.34 (m, 8H), 0.91 (t, *J* = 6.8 Hz, 6H), 0.39 (s, 3H); ¹³C NMR (CDCl₃, 100 MHz) δ 144.1, 139.2, 136.8, 134.6, 131.1, 130.9, 130.7, 114.3, 108.0, 31.7, 31.5, 31.0, 29.8, 22.8, 14.3, -0.2; HRMS (*m/z*, ESI, [M+Na]⁺) Calcd for C₃₆H₄₆⁷⁹Br₄S₄Si₂Na 1000.8652, found 1000.8654; calcd for C₃₆H₄₆⁷⁹Br₃⁸¹BrS₄Si₂Na 1002.8632, found 1002.8639; calcd for C₃₆H₄₆⁷⁹Br₂⁸¹Br₂S₄Si₂Na 1004.8611, found 1004.8623; calcd for C₃₆H₄₆⁷⁹Br⁸¹Br₃S₄Si₂Na 1006.8591, found 1006.8597; calcd for C₃₆H₄₆⁸¹Br₄S₄Si₂Na 1008.8570, found 1008.8573.

Synthesis of 5,11-dihexyl-4,4,10,10-tetraoctyl-2,8-bis(trimethylsilyl)benzo[1,2-b:4,5-b']bis-thieno[4'',5''-b''':4''',5'''-b''']silolo[2'',3''-d:2''',3'''-d']thiophene (TMS-ARSi, 5): To **4** (3.93 g, 4.0 mmol) in anhydrous THF (120 mL) was added *t*-BuLi (1.64 M in pentane, 20.00 mL, 32.4 mmol) at -90 °C under argon atmosphere and then stirred for 2h. A solution of dichlorodioctylsilane (3.60 mL, 10.4 mmol) in anhydrous THF (10.40 mL) was added dropwise into the reaction mixture at low temperature, then the reactant was allowed to slowly

warm to room temperature overnight while maintaining stirring. The reactant was quenched by addition of water, and extracted with hexane. The combined extracts was washed with brine, dried over anhydrous MgSO_4 , and then filtrated. The solvent was removed by rotary evaporation, and the crude product was purified by column chromatography on silica gel with hexane as eluent to afford **5** as a sticky orange liquid (3.13 g, 67 %). ^1H NMR (CDCl_3 , 400 MHz) δ 7.22 (s, 2H), 3.13 (t, $J = 8.4$ Hz, 4H), 1.84 (m, 4H), 1.61-1.57 (m, 4H), 1.43-1.12 (m, 64H), 0.97 (t, $J = 6.8$ Hz, 6H), 0.87 (t, $J = 6.8$ Hz, 12H), 0.40 (s, 18H); ^{13}C NMR (CDCl_3 , 100 MHz) δ 154.5, 148.6, 143.7, 142.4, 141.5, 138.4, 136.5, 134.7, 129.5, 35.8, 33.3, 32.0, 31.9, 30.4, 29.6, 29.3, 29.2, 24.3, 22.9, 22.8, 14.3, 14.2, 13.1, 0.4; HRMS (m/z , ESI, $[\text{M}+\text{Na}]^+$) Calcd for $\text{C}_{68}\text{H}_{114}\text{S}_4\text{Si}_4\text{Na}$ 1193.6778, found 1198.6769.

Synthesis of 2,8-dibromo-5,11-dihexyl-4,4,10,10-tetraoctylbenzo[1,2-b:4,5-b']bis-thieno[4'',5''-b'':4''',5'''-b''']silolo[2'',3''-d:2''',3'''-d']thiophene (Br-ARSi, 6): A solution of *N*-bromosuccinimide (934 mg, 5.25 mmol) in anhydrous THF (100 mL) was added dropwise into a solution of **5** (2.93 g, 2.50 mmol) in anhydrous THF (100 mL) at 0 °C with the absence of light. The reactant was stirred overnight and slowly warmed to room temperature, followed by extraction with water and hexane. The combined extracts was washed with brine, dried over anhydrous MgSO_4 , and then filtrated. The solvent was removed by rotary evaporation, and the crude product was purified by column chromatography on silica gel with hexane as eluent to afford **6** as a sticky orange liquid (2.16 g, 73 %). ^1H NMR (CDCl_3 , 400 MHz) δ 7.09 (s, 2H), 3.08 (t, $J = 8.4$ Hz, 4H), 1.81-1.78 (m, 4H), 1.58 (m, 4H), 1.40-1.09 (m, 64H), 0.95 (t, $J = 6.8$ Hz, 6H), 0.83 (t, $J = 6.8$ Hz, 12H); ^{13}C NMR (CDCl_3 , 100 MHz) δ 149.8, 148.2, 142.7, 141.6, 138.3, 133.6, 132.5, 129.7, 112.5, 35.7, 33.2, 31.9, 31.8, 30.3, 29.5, 29.2, 29.0, 24.1, 22.8, 22.6, 14.1, 14.0, 12.7; HRMS m/z , ESI, $[\text{M}+\text{Na}]^+$) Calcd for $\text{C}_{62}\text{H}_{96}^{79}\text{Br}_2\text{S}_4\text{Si}_2\text{Na}$ 1205.4198, found 1205.4179; calcd for $\text{C}_{62}\text{H}_{96}^{79}\text{Br}^{81}\text{BrS}_4\text{Si}_2\text{Na}$ 1207.4177, found 1205.4125;

clad for $C_{62}H_{96}^{81}Br_2S_4Si_2Na$ 1209.4157, found 1209.4110.

Synthesis of 5,11-dihexyl-4,4,10,10-tetraoctyl-2,8-bis(trimethylstannyl)benzo[1,2-b:4,5-b']bis-thieno[4'',5''-b''':4''',5'''-b''']silolo[2'',3''-d:2''',3'''-d']thiophene (Sn-ARSi, 7): A solution of **6** (783 mg, 0.66 mmol) in anhydrous THF (66 mL) was added dropwise *t*-BuLi (1.64 M in pentane, 1.69 mL, 2.77 mmol) at -90 °C under argon atmosphere and then stirred for 1h. Trimethyltin chloride solution (1 M in hexane, 2.90 mL, 2.90 mmol) was subsequently added in one portion into the reaction mixture. The reactant was stirred overnight and slowly warmed to room temperature, quenched with water and extracted with hexane. The combined extracts was washed with brine, dried over anhydrous $MgSO_4$, and then filtrated. The solvent was removed by rotary evaporation to afford **7** as sticky orange oil and used without further purifications (812 mg, 91 %).

*Synthesis of 4,7-Dibromobenzo[*c*][1,2,5]oxadiazole (DiBr-BO):* This compound was prepared according to the literature procedure.^[3] 1H NMR ($CDCl_3$, 400 MHz) δ 7.49 (s, 2H); ^{13}C NMR ($CDCl_3$, 100 MHz) δ 149.4, 134.2, 180.7.

*Synthesis of Naphtho[1,2-*c*:5,6-*c'*]-bis[1,2,5]oxadiazole (NO):* 5% Sodium hypochlorite solution (21 mL) was dropwise added to a stirred, cooled solution of 1,5-dinitronaphthalene-2,6-diamine (2.0 g, 6.4 mmol) in 1 M alcoholic sodium hydroxide (300 mL) at 0 °C. The mixture was stirred at this temperature for an additional 30 min. Then, most ethanol was removed under reduced pressure, and the residue was filtered and washed with sufficient amount of water to afford **NO**'s dioxide as dark yellow solid. The **NO**'s dioxide could be used in the following reaction without further purification and drying. A mixture of **NO**'s dioxide, PPh_3 (4.8 g, 18.3 mmol) and THF (20 mL) was charged under nitrogen and stirred at 80 °C for 30 h until the starting material is consumed (TLC). After cooling to room temperature, the

solution was removed under reduced pressure, and the residue was dissolved in CH_2Cl_2 , washed with water, dried over MgSO_4 , concentrated to give a crude product. The residue was washed with ethanol to give the pure compound (0.58 g, 43 %). ^1H NMR (CDCl_3 , 400 MHz) δ 8.51 (d, $J = 9.2$ Hz, 2H), 8.07 (d, $J = 9.2$ Hz, 2H); ^{13}C NMR (CDCl_3 , 100 MHz) δ 148.9, 147.5, 128.7, 122.9, 117.4; HRMS (m/z , FAB^+) Calcd for $\text{C}_{10}\text{H}_4\text{N}_4\text{O}_2$ 212.0334, found 212.0332.

Synthesis of 4,9-dibromonaphtho[1,2-c:5,6-c']-bis[1,2,5]oxadiazole (DiBr-NO): Compound **NO** (0.37 g, 1.75 mmol) and NBS (0.93 g, 5.23 mmol) were dissolved in a mixed solvent of sulfuric acid (7 mL) and trifluoroacetic acid (21 mL). The solution was stirred at room temperature overnight. Then the mixture was poured into ice water carefully, and the crude product was precipitated and collected by filtration. The residue was washed with water, ethanol and chloroform to give the pure compounds (0.31 g, 48 %). ^1H NMR (CDCl_3 , 400 MHz) δ 8.67(s, 2H). ^{13}C NMR could not be recorded due to the low solubility of **DiBr-NO**. HRMS (m/z , FAB^+) Calcd for $\text{C}_{10}\text{H}_2^{79}\text{Br}_2\text{N}_4\text{O}_2$ 367.8545, found 367.8549; calcd for $\text{C}_{10}\text{H}_2^{79}\text{Br}^{81}\text{BrN}_4\text{O}_2$ 369.8524, found 369.8530; calcd for $\text{C}_{10}\text{H}_2^{81}\text{Br}_2\text{N}_4\text{O}_2$ 371.8504, found 371.8512.

General procedures of polymerization: Ditin-monomer (0.3 mmol), dibromo-monomer (0.3 mmol), tri(*o*-tolyl)phosphine (16 mol% with respect to the ditin-monomer), and tris(dibenzylideneacetone)dipalladium(0) (2 mol% with respect to the ditin-monomer) were dissolved in degassed chlorobenzene (5 mL). Then, the copolymer was synthesized *via* microwave-assisted Stille polycondensation (150 °C for 30 min). After end-capping with trimethyl(thiophen-2-yl)stannane and 2-bromothiophene (both 1.1 equiv. with respect to the monomers and under microwave heating at 160 °C, 10 min for each process), the mixture was

cooled and poured into methanol to afford a solid precipitate. The crude polymer was extracted using the Soxhlet apparatus with methanol, acetone, hexane, CH_2Cl_2 , and chloroform. The polymers extracted from solvents were precipitated in methanol and dried overnight under vacuum at 60 °C.

PSiBO. Compound **DiBr-BO** was selected as the dibromo-monomer for polymerization. Hexane extracted most of polymer in the Soxhlet apparatus to give **PSiBO** as brown solid (315 mg, 92 %). GPC: $M_n = 61.8$ kDa, $M_w = 172.8$ kDa, PDI = 2.8. ^1H NMR (d_2 -1,1,2,2-tetrachloroethane, 400 MHz) δ 8.71 (s, 2H), 7.75 (s, 2H), 2.28-0.74 (bm, 94H).

PSiNO. Compound **DiBr-NO** was selected as the dibromo-monomer for polymerization of **PSiNO**. Chloroform extracted most of polymer in the Soxhlet apparatus (203 mg, 48 %). GPC: $M_n = 100.4$ kDa, $M_w = 151.4$ kDa, PDI = 1.5. ^1H NMR (400 MHz, d_2 -1,1,2,2-tetrachloroethane, ppm): $\delta = 8.07$ (bm, 4H), 3.17-0.66 (bm, 94H).

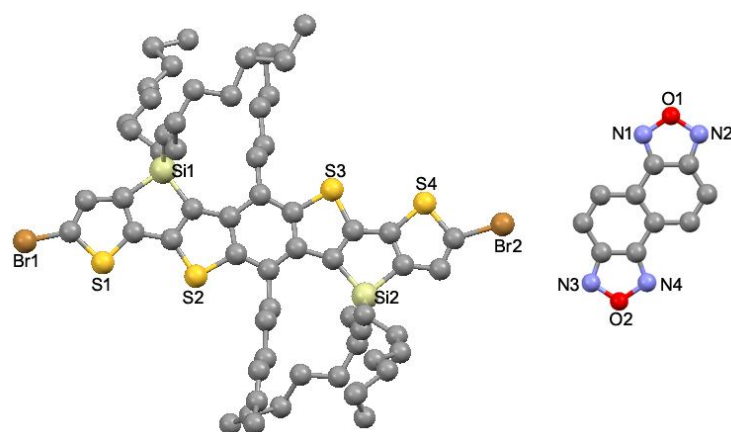


Fig. S1 Single-crystal X-ray structures of dibromo-ARSi (**6**) and NO. Hydrogen atoms are removed for clarity.

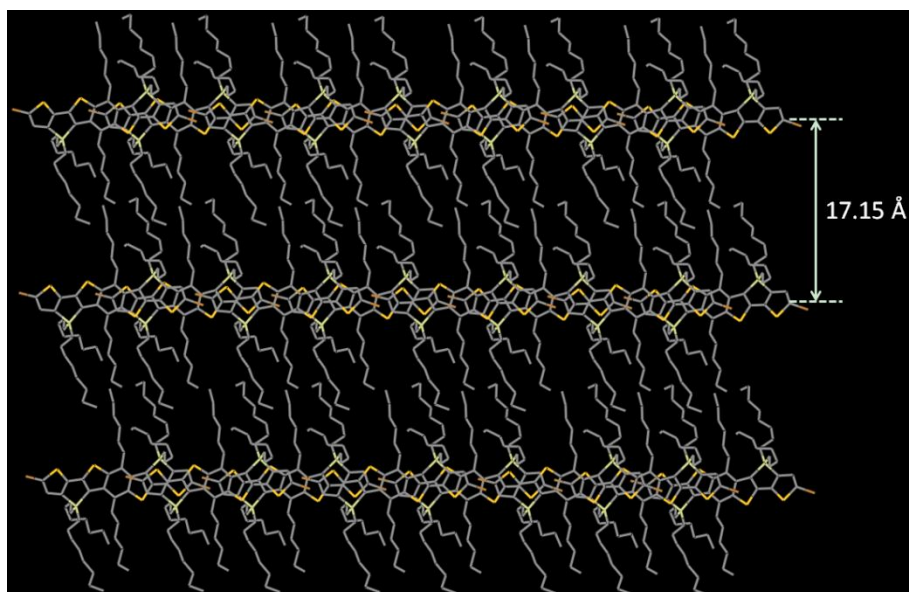


Fig. S2 Crystal packing diagram of dibromo-ARSi (6).

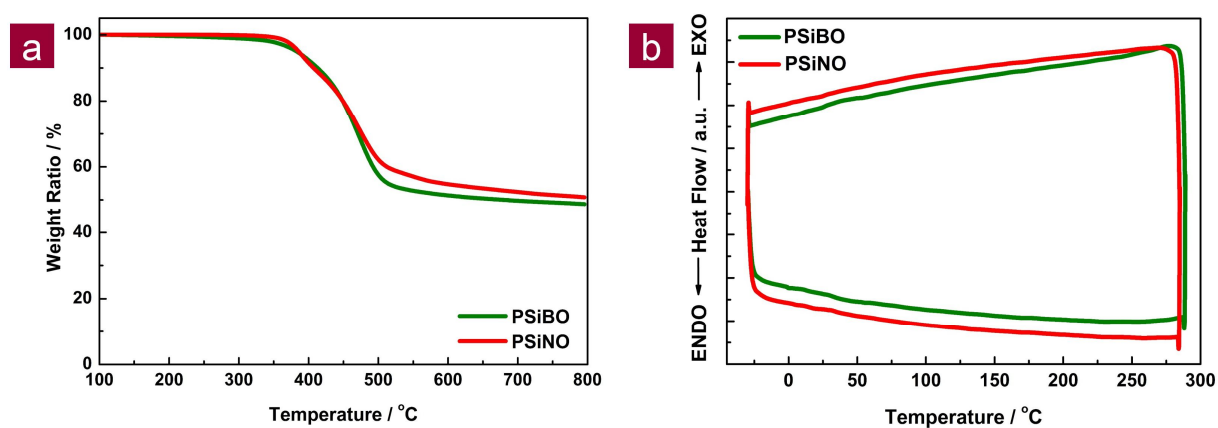


Fig. S3 a) Thermogravimetric analysis (ramp rate: $10\text{ }^{\circ}\text{C min}^{-1}$) of PSiNO and PSiBO copolymers. The purge gas for TGA was nitrogen. The onset decomposition temperatures of PSiNO and PSiBO at 5% weight loss are 386 and 383 $^{\circ}\text{C}$, respectively. b) DSC curve of the studied copolymers.

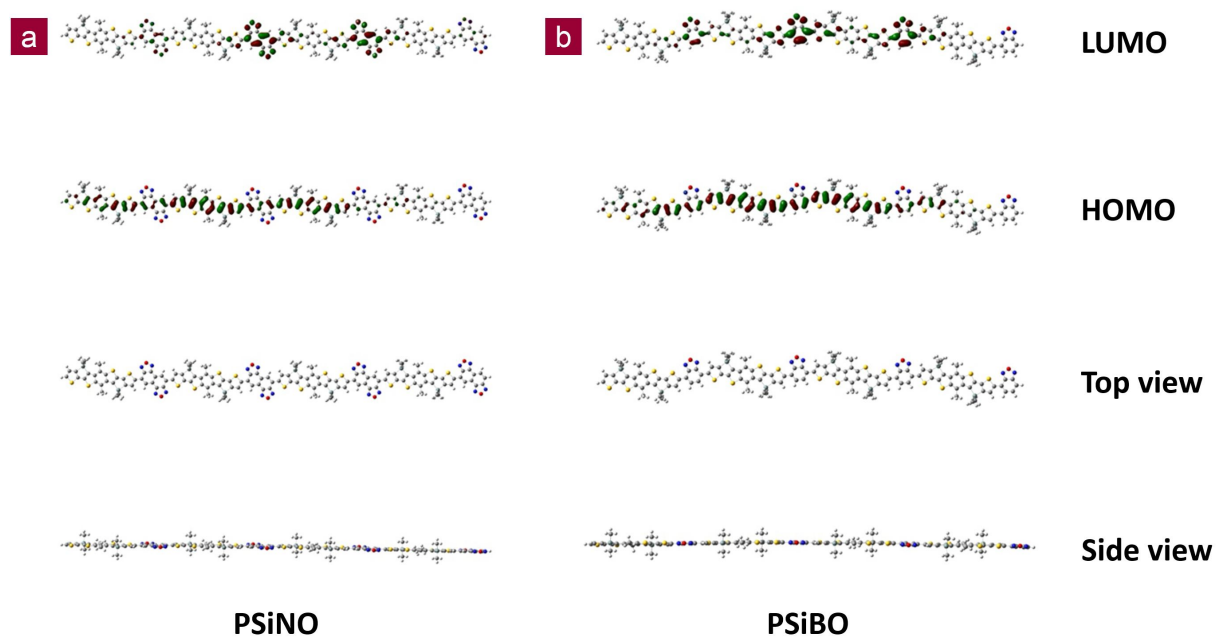


Fig. S4 Minimum energy conformations of tetramers of PSiNO and PSiBO. Gaussian optimized at B3LYP/6-31G* level with visualization of the corresponding HOMO/LUMO energy distributions.

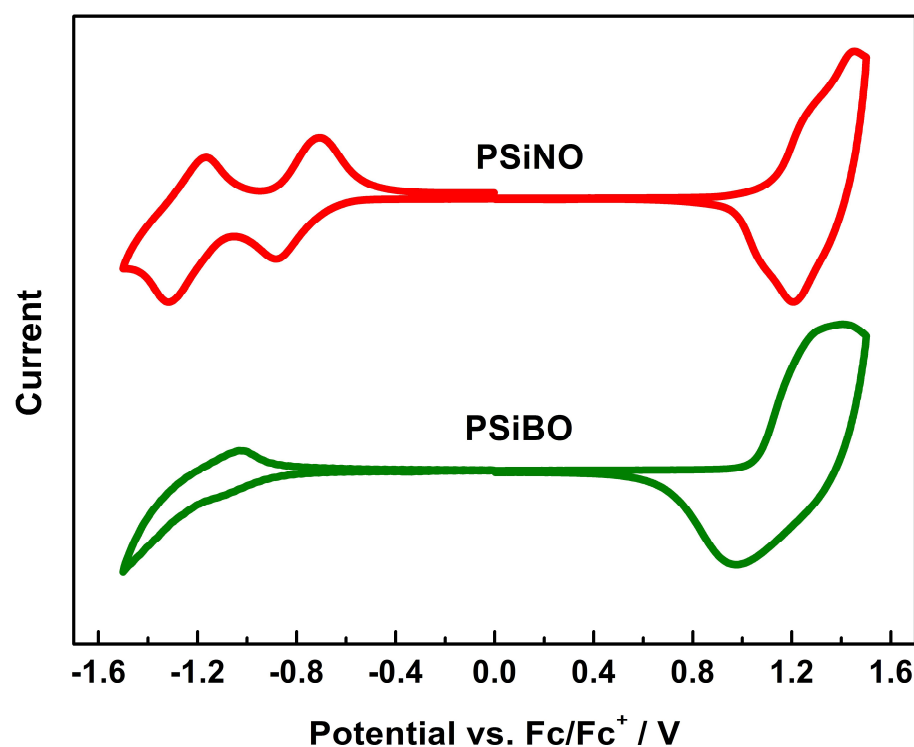


Fig. S5 Cyclic voltammograms of the polymer films on platinum electrode in 0.1 mol L⁻¹ Bu₄NPF₆ acetonitrile solution at a scan rate of 50 mV s⁻¹.

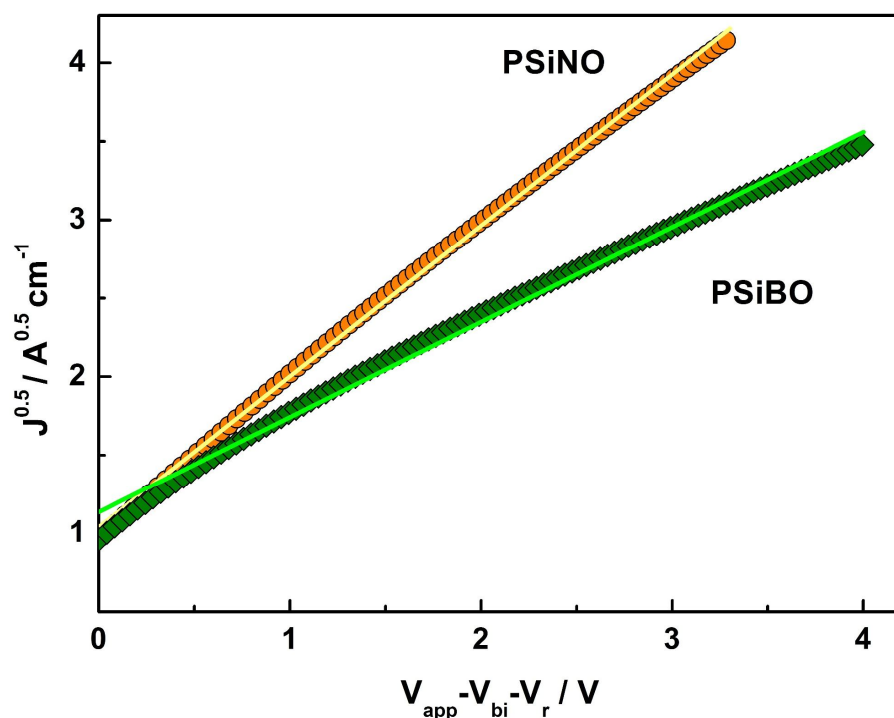


Fig. S6 Determination of the hole mobility from the dark current densities for the pristine PSiNO and PSiBO polymers.

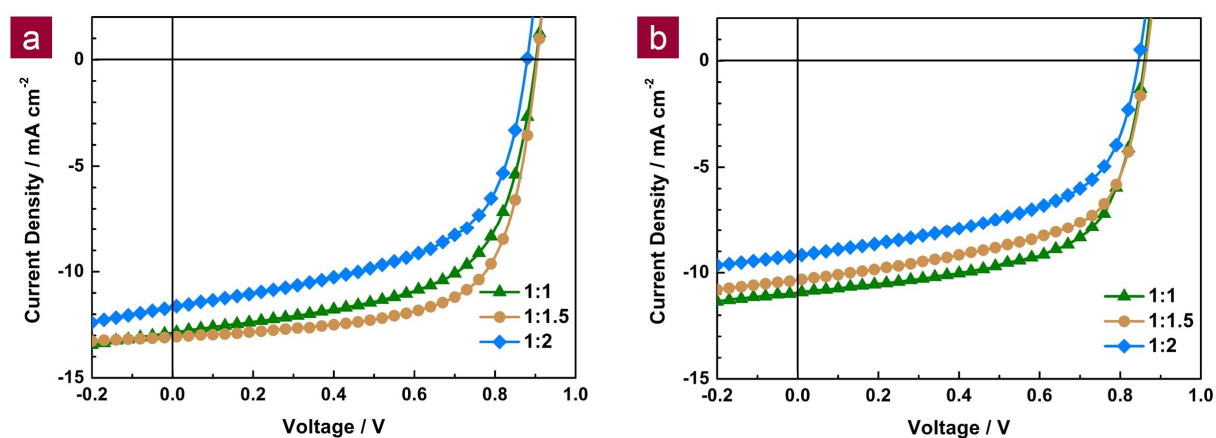


Fig. S7 Current density versus voltage (J - V) characteristics of optimized devices made from various blend ratios of a) PSiNO:PC₇₁BM with 0.5% 1,8-diiodooctane (DIO) adopted as an additive and b) PSiBO:PC₇₁BM with 3% DIO under AM1.5 white light illumination at 100 mW cm⁻².

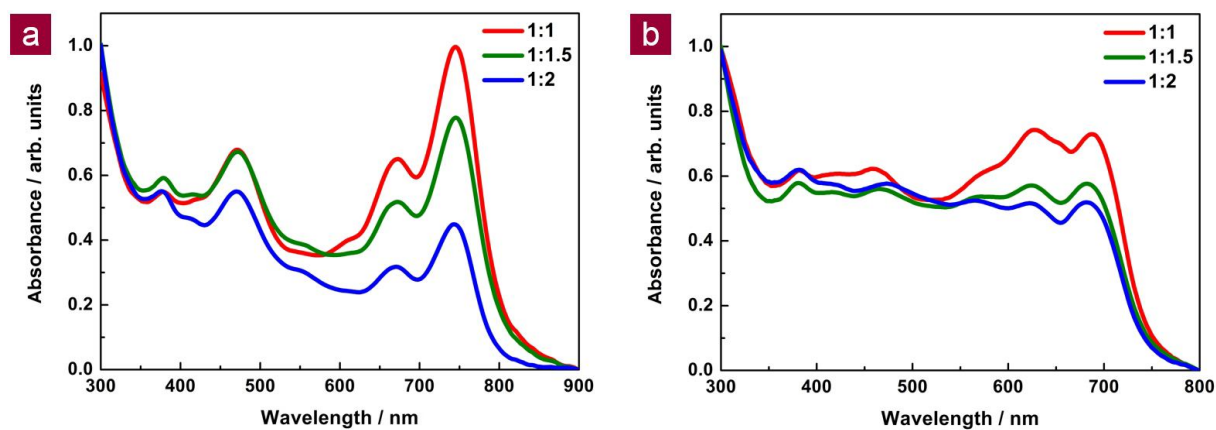


Fig. S8 UV-vis spectra of a) PSiNO:PC₇₁BM and b) PSiBO:PC₇₁BM blend films.

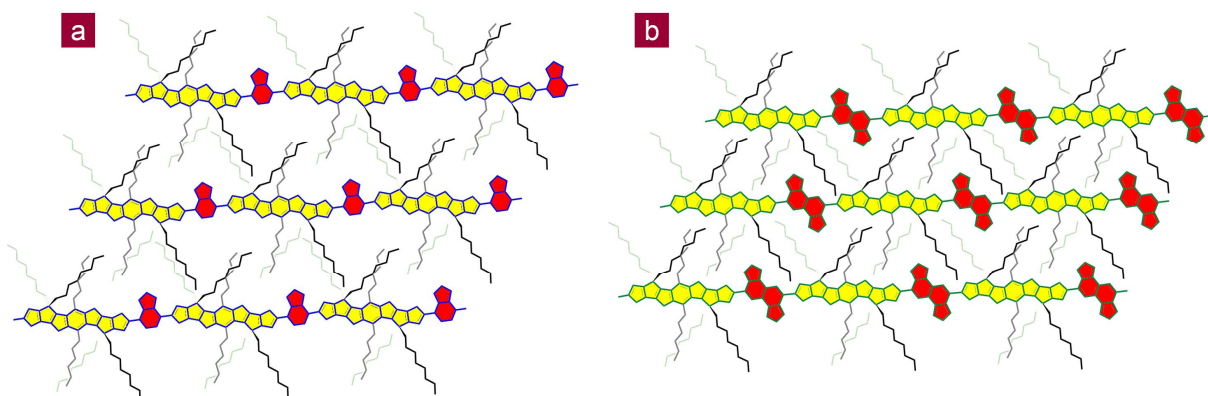


Fig. S9 Schematic illustration of alkyl side-chains interdigitating and/or tilting out of the a) PSiBO and b) PSiNO polymer backbone plane in the solid state.

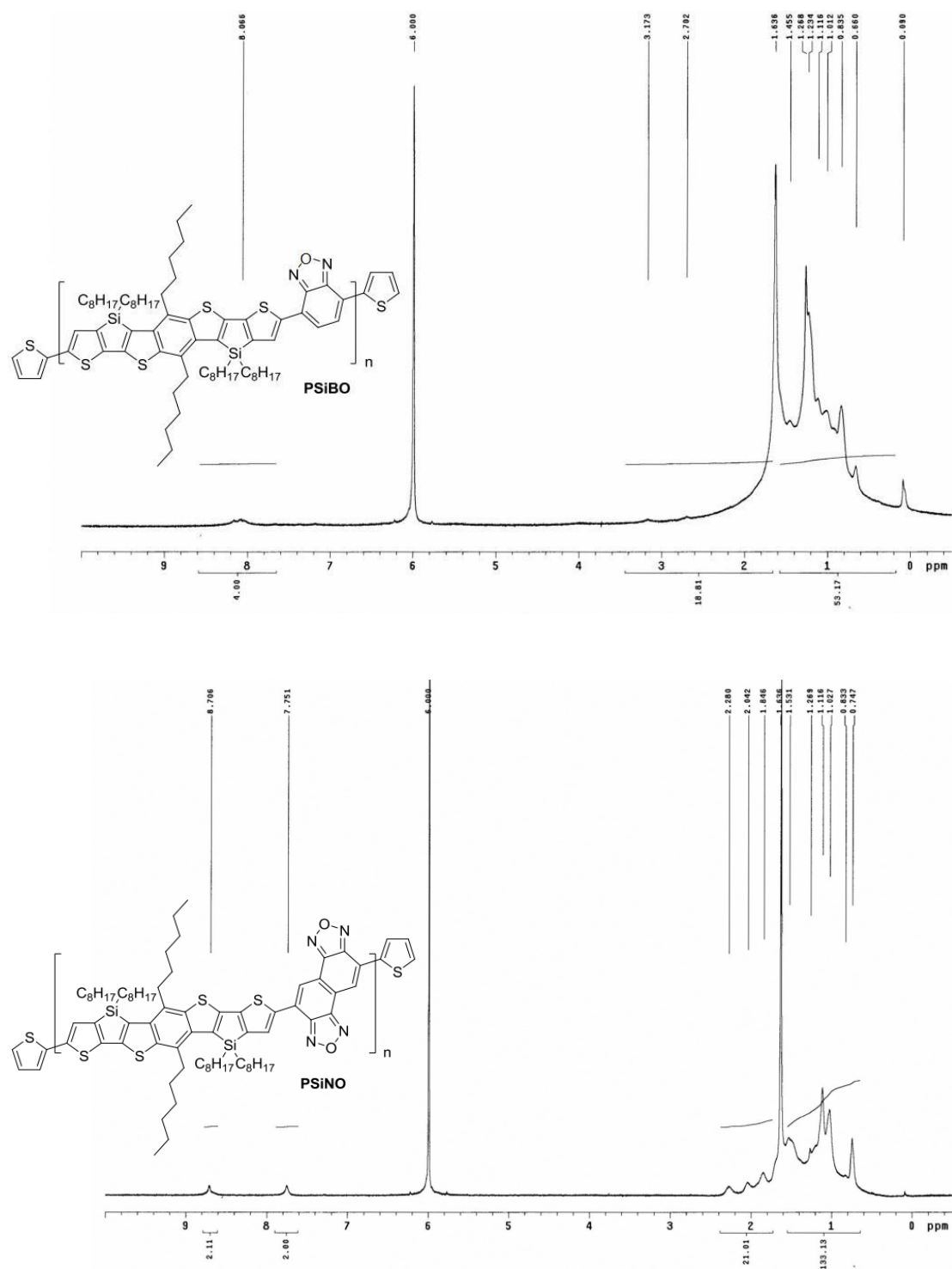


Fig. S10 ^1H NMR spectra of two polymers **PSiBO** and **PSiNO**.

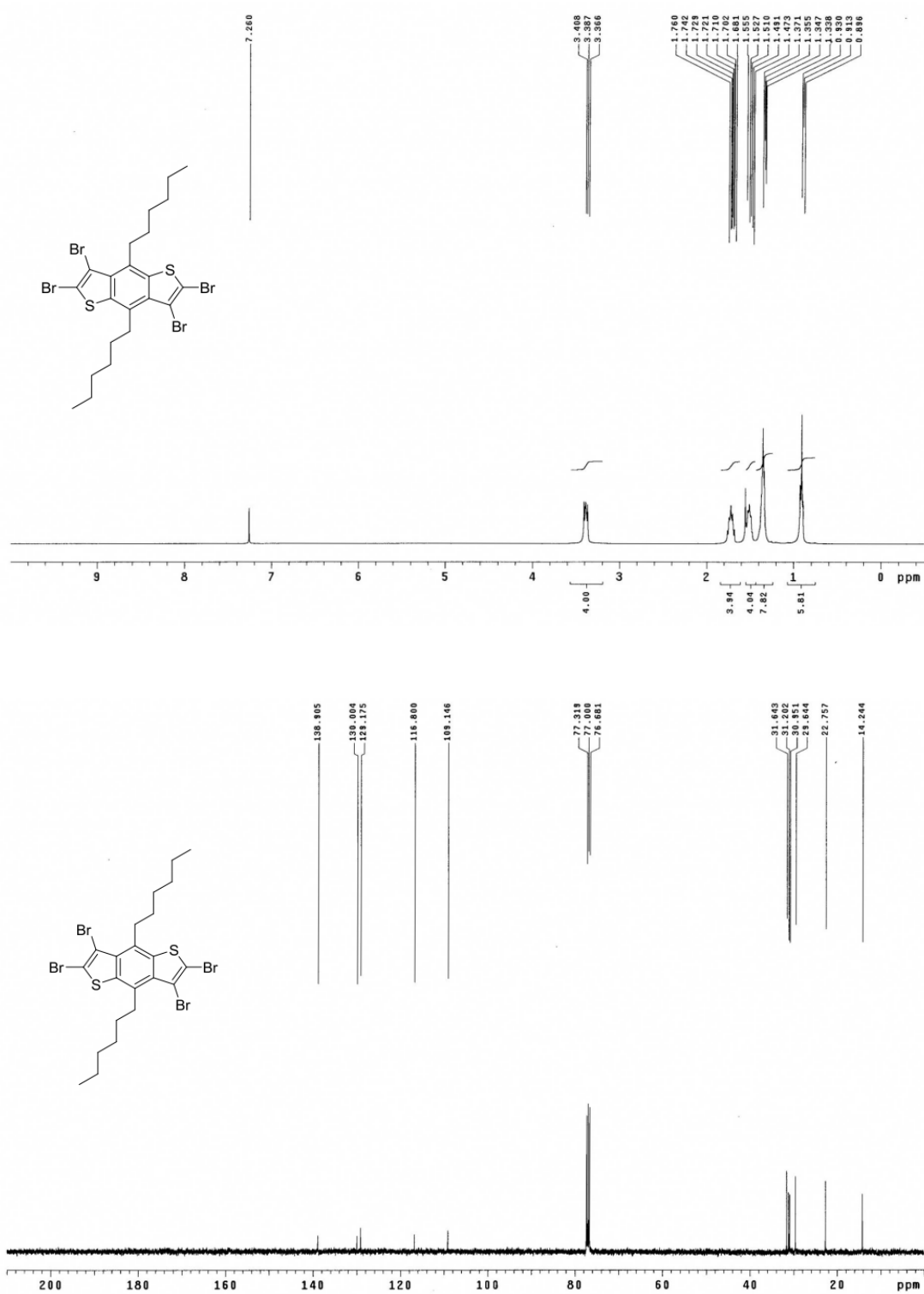


Fig. S11 ^1H NMR and ^{13}C NMR spectra of compound 2.

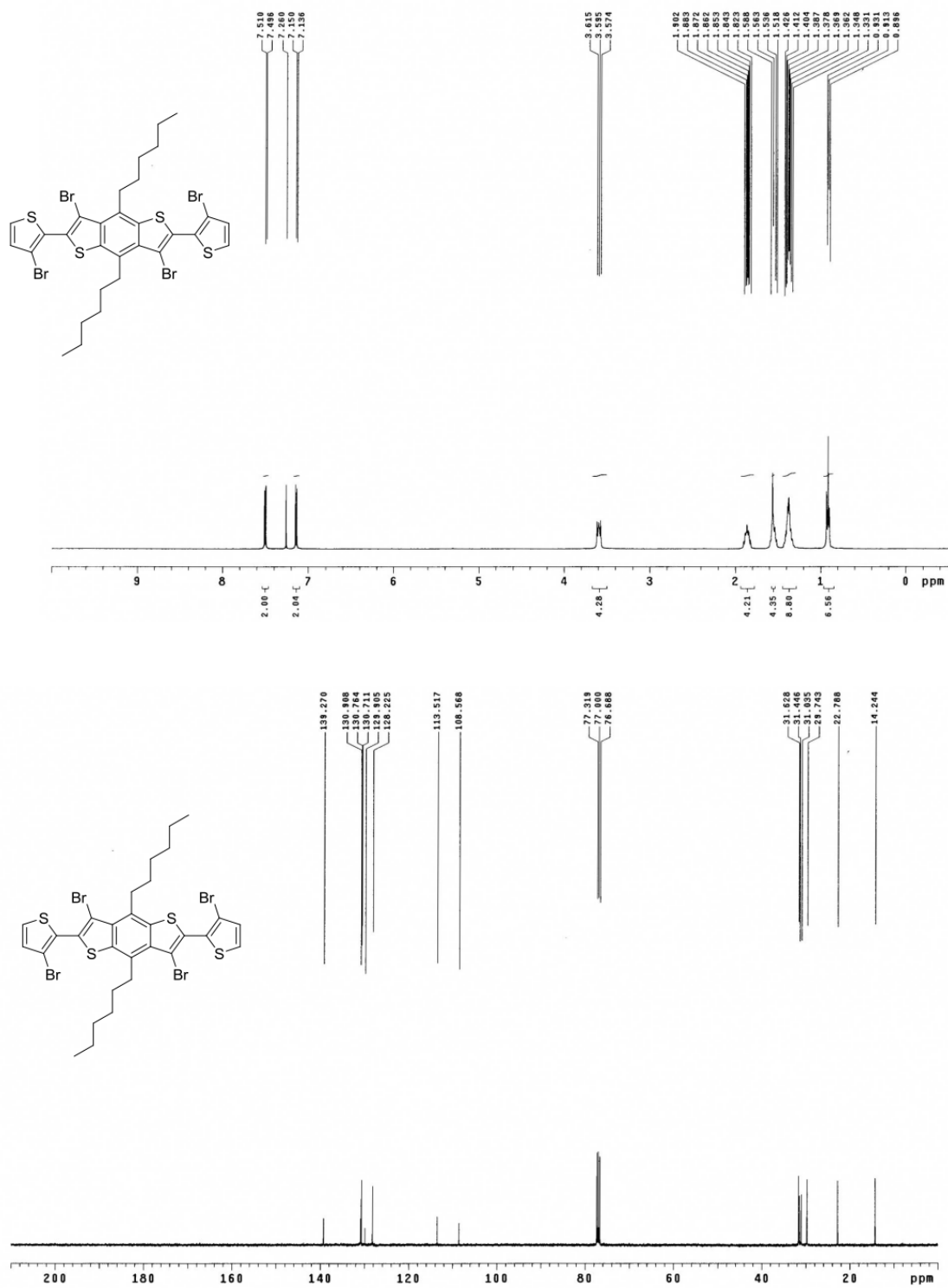


Fig. S12 ^1H NMR and ^{13}C NMR spectra of compound 3.

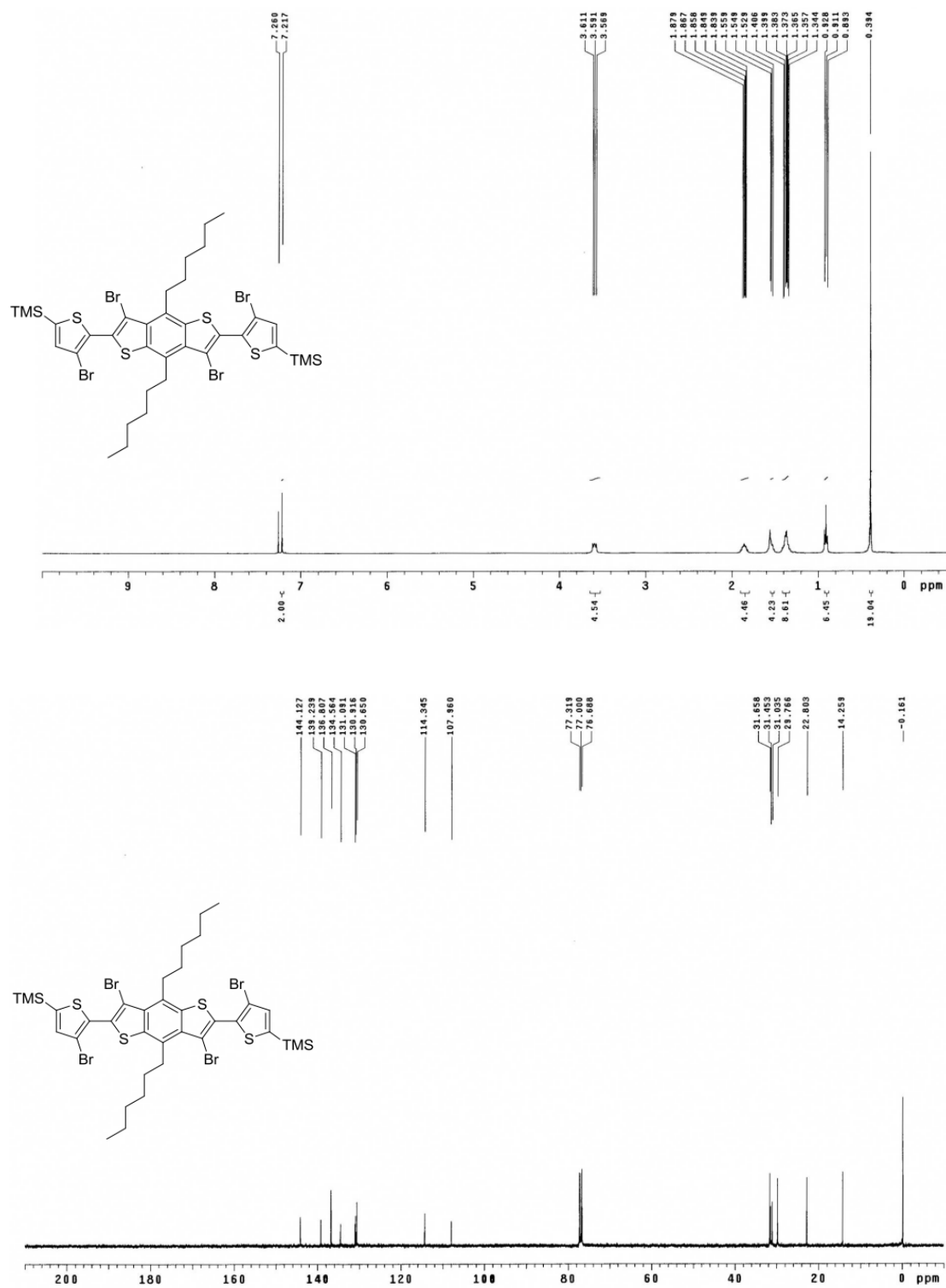


Fig. S13 ^1H NMR and ^{13}C NMR spectra of compound 4.

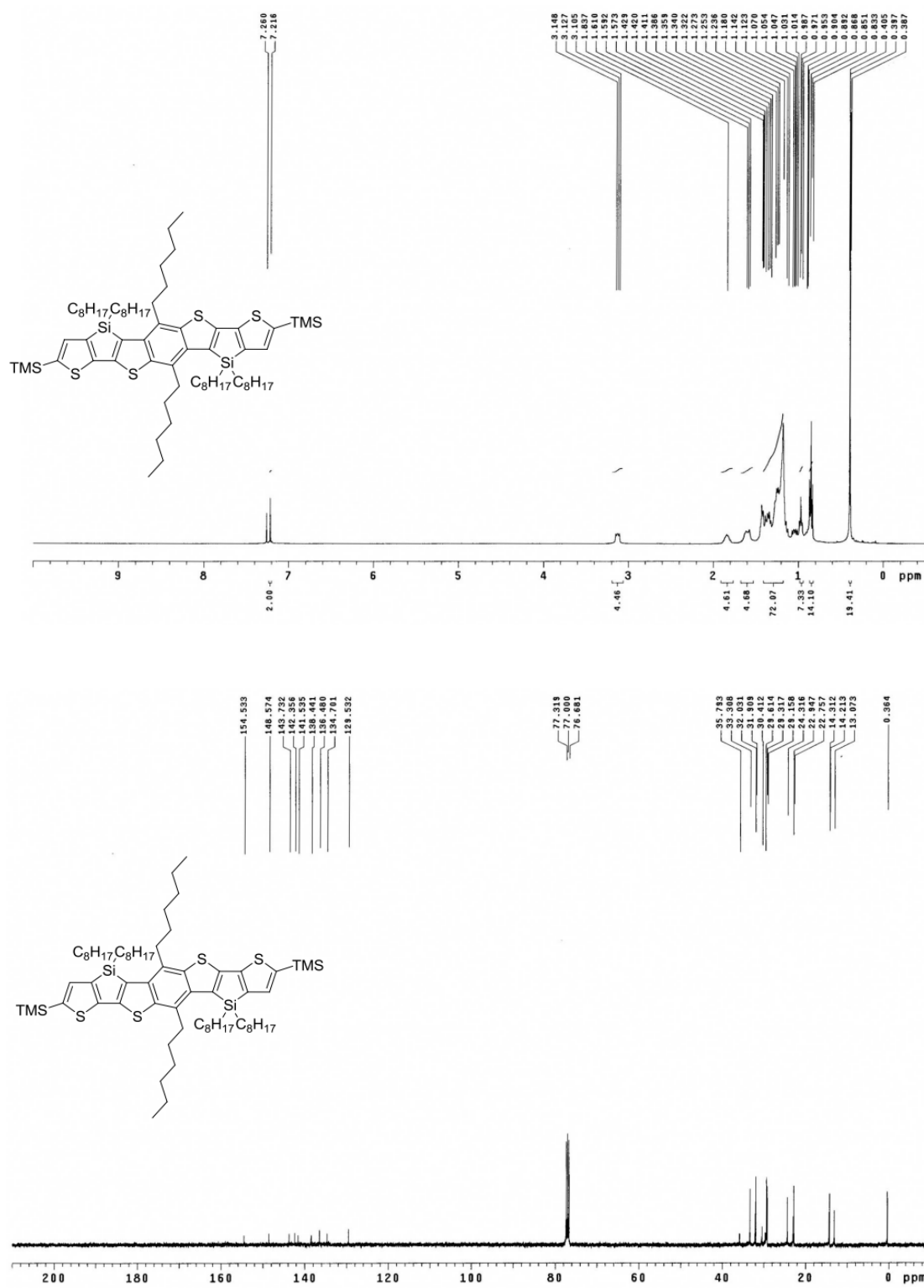


Fig. S14 ^1H NMR and ^{13}C NMR spectra of compound 5.

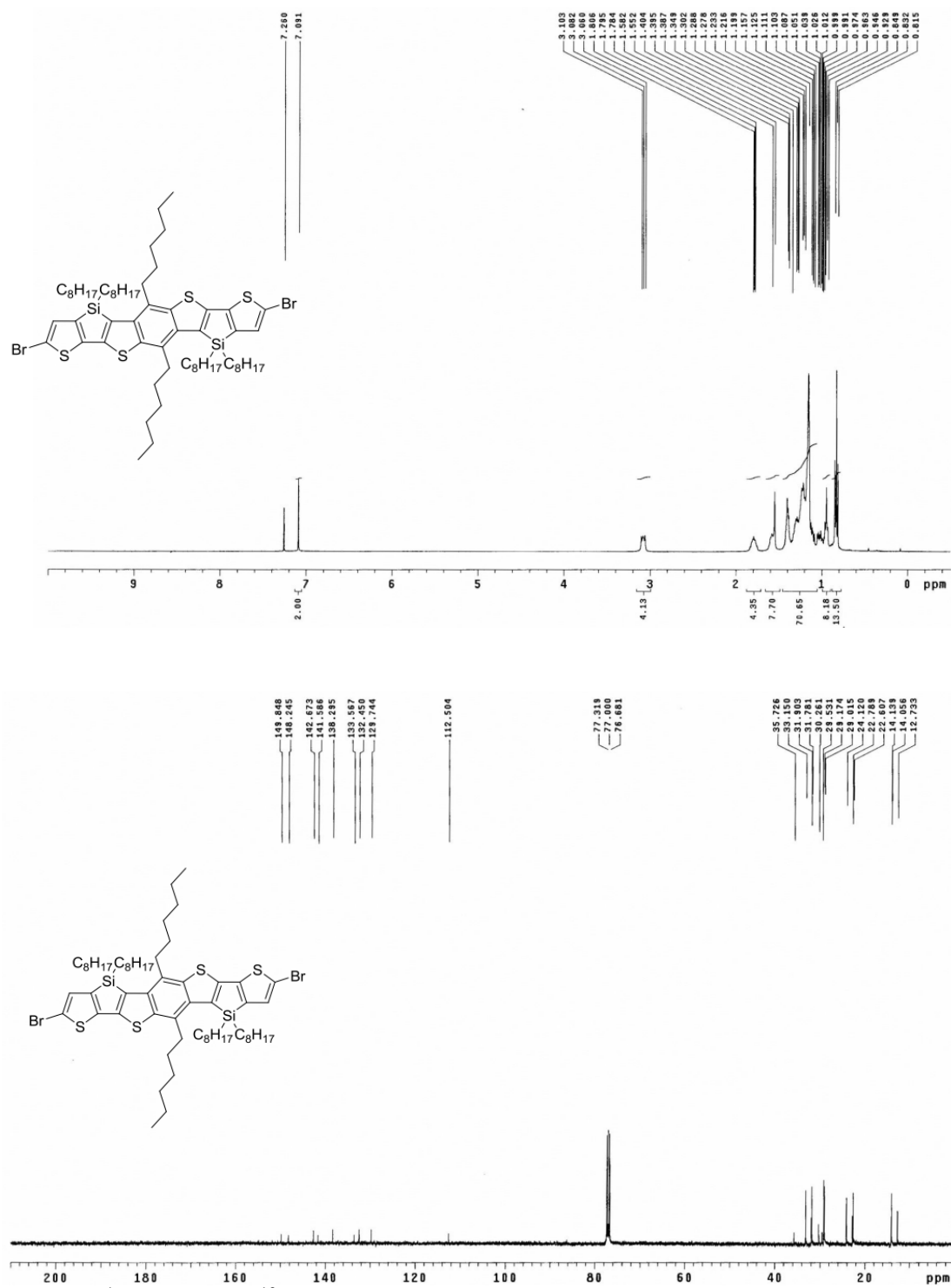


Fig. S15 ^1H NMR and ^{13}C NMR spectra of compound 6.

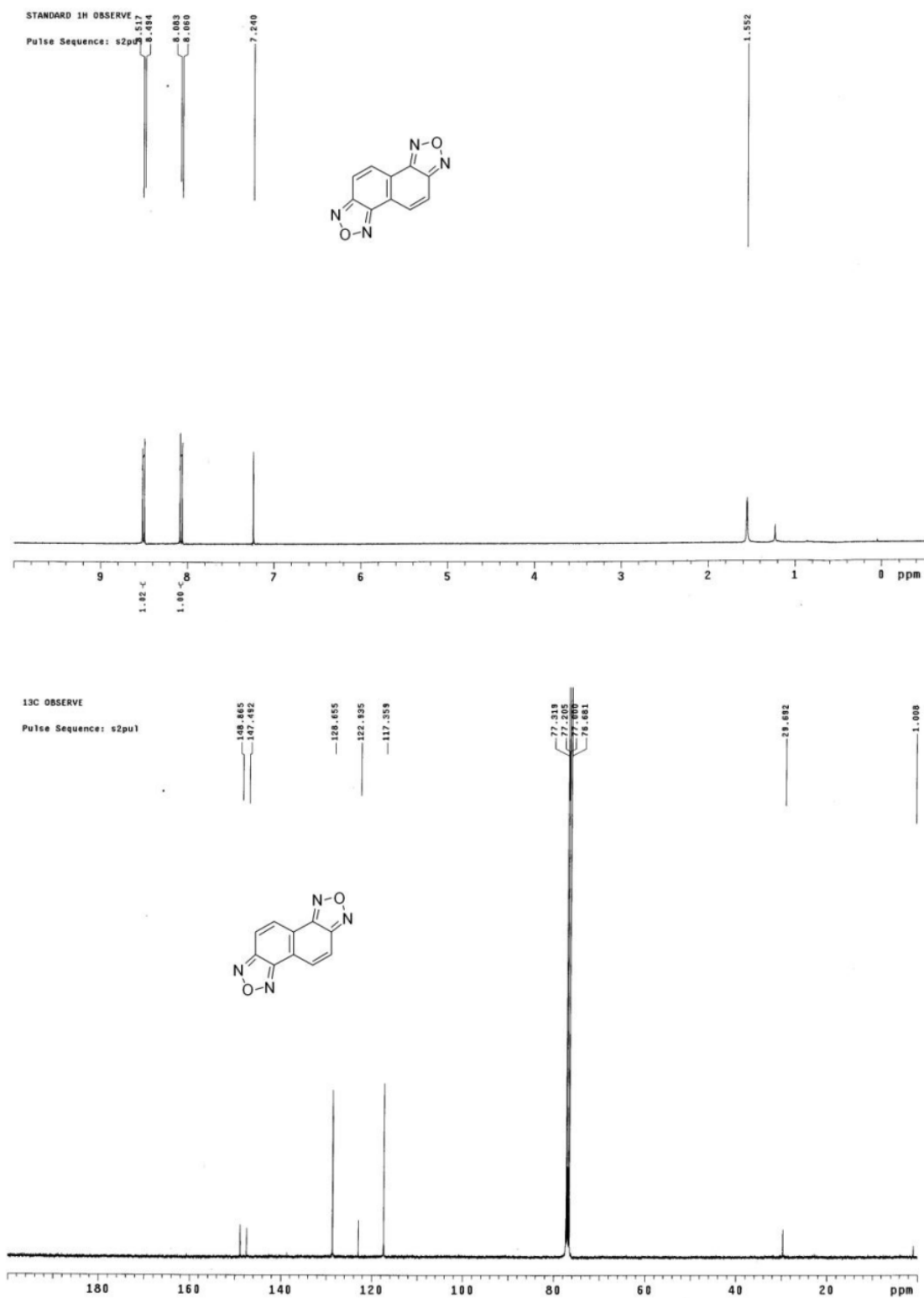


Fig. S16 ¹H NMR and ¹³C NMR spectra of NO.

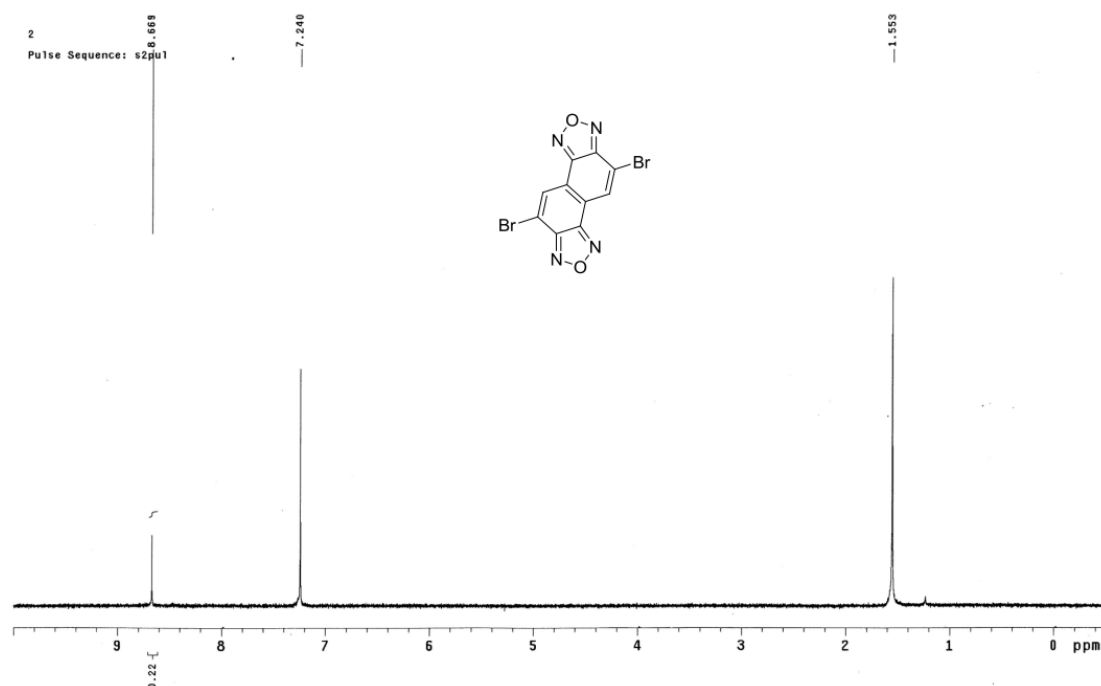


Fig. S17 ^1H NMR spectra of DiBr-NO.

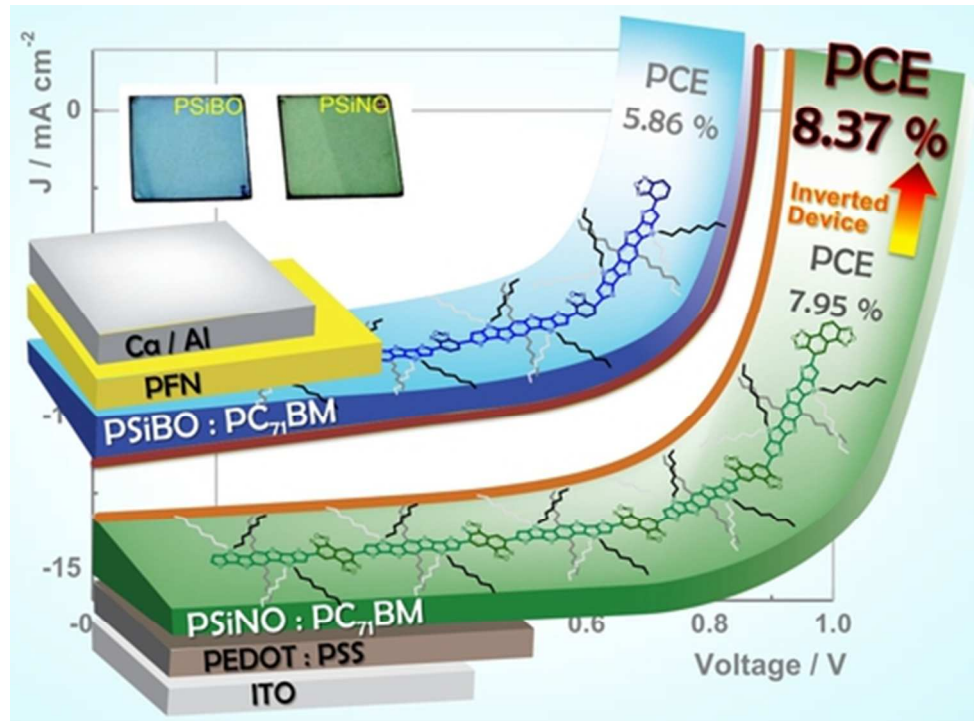
Table S1 Crystal data and structure refinement for compounds **6** and NO.

	6	NO
CCDC NO.	1014680	1013475
Empirical formula	C ₆ H ₉ Br ₂ S ₄ Si ₂	C ₁₀ H ₄ N ₄ O ₂
Formula weight	1185.63	212.17
Temperature	295(2) K	150(2) K
Wavelength	1.54178 Å	0.71073 Å
Crystal system	Triclinic	Monoclinic
Space group	P1	P2(1)/n
Unit cell dimensions	a = 9.6261(4) Å α = 92.491(5) $^\circ$ b = 10.7307(6) Å β = 98.119(5) $^\circ$ c = 17.4242(11) Å γ = 108.490(5) $^\circ$	a = 3.7449(3) Å α = 90 $^\circ$ b = 6.5953(5) Å β = 93.931(2) $^\circ$ c = 17.3411(14) Å γ = 90 $^\circ$
Volume	168.33(16) Å ³	427.30(6) Å ³
Z	1	2
Density (calculated)	1.170 mg/m ³	1.649 mg/m ³
Absorption coefficient	3.273 mm ⁻¹	0.122 mm ⁻¹
F(000)	630	216
Crystal size	0.20 x 0.10 x 0.10 mm ³	0.50 x 0.25 x 0.08 mm ³
Theta range for data collection	4.36 to 67.99 $^\circ$	2.35 to 27.48 $^\circ$
Index ranges	-11 \leq h \leq 9, -11 \leq k \leq 12, -20 \leq l \leq 20	-4 \leq h \leq 4, -8 \leq k \leq 8, -22 \leq l \leq 22
Reflections collected	14644	3681
Independent reflections	7675 [R(int) = 0.0316]	974 [R(int) = 0.0312]

Completeness to theta = 27.50°	99.8 %	100.0 %
Absorption correction	None	Semi-empirical from equivalents
Max. and min. transmission	1.00000 and 0.86597	0.9903 and 0.9415
Refinement method	Full-matrix least-squares on F ²	Full-matrix least-squares on F ²
Data / restraints / parameters	7675 / 477 / 538	974 / 0 / 73
Goodness-of-fit on F ²	1.133	1.122
Final R indices [I>2sigma(I)]	R1 = 0.0607, wR2 = 0.1696	R1 = 0.0473, wR2 = 0.1220
R indices (all data)	R1 = 0.1101, wR2 = 0.2140	R1 = 0.0552, wR2 = 0.1289
Largest diff. peak and hole	0.484 and -0.285 e.Å ⁻³	0.269 and -0.256 e.Å ⁻³

Reference:

- [1] V. D. Mihailetchi, H. Xie, B. de Boer, L. J. A. Koster and P. W. M. Blom, *Adv. Funct. Mater.*, 2006, **16**, 699-708.
- [2] Z. He, C. Zhong, X. Huang, W.-Y. Wong, H. Wu, L. Chen, S. Su and Y. Cao, *Adv. Mater.*, 2011, **23**, 4636.
- [3] X. Wang, P. Jiang, Y. Chen, H. Luo, Z. Zhang, H. Wang, X. Li, G. Yu and Y. Li, *Macromolecules*, 2013, **46**, 4805.



20x15mm (600 x 600 DPI)